NAS5-30312

Development of a Unique Laboratory Standard Indium Gallium Arsenide Detector for the 500 - 1700 nm Spectral Region

NASA Phase II Final Report

May 31, 1990

ORIGINAL PAGE
COLOR PHOTOGRAPH

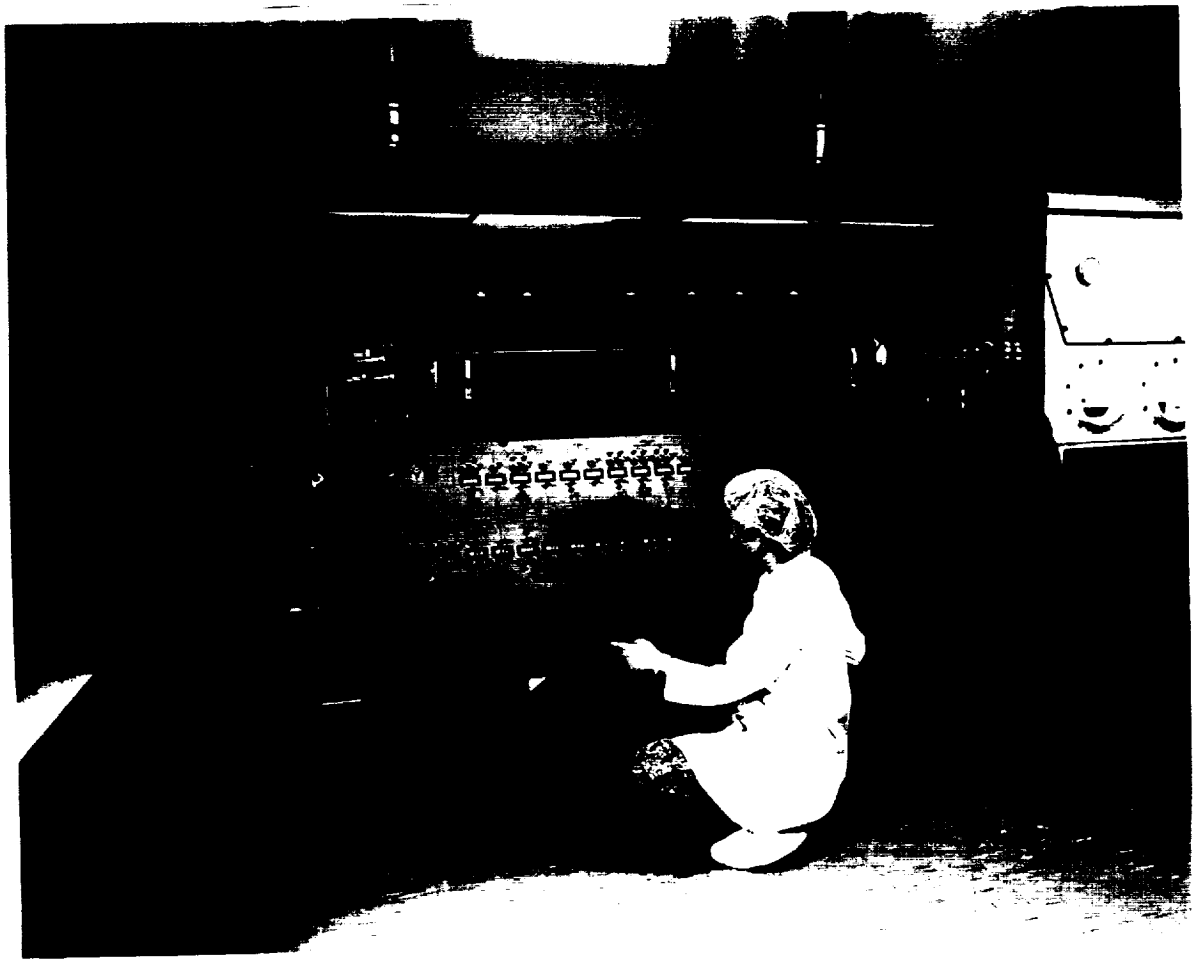

EPITAXX, Inc.
3490 U.S. Route One
Princeton, NJ 08540
(609) 452-1188

Abstract

In the course of this work, we produced 5 mm diameter InGaAs pin detectors which met or exceeded all of the goals proclaimed at the onset of the program.

The best results achieved were:

* Shunt resistance of over 300 K ohms
* Rise time of less than 300 ns
* Contact resistance of less than 20 ohms
* Quantum efficiency of over 50% in the 0.5 - 1.7 um range
* Devices were maintained and operated at 125°C without deterioration for over 100 hours

The above values meet or exceed the goals of the program. Ten operational, fully characterized detectors are delivered with this report.

In order to achieve the goals of this program, several major technological advances were realized, among them:

* Successful design, construction and operation of a hydride VPE reactor capable of growing epitaxial layers on 2" diameter InP substrates with a capacity of over 8 wafers per day.

* Wafer processing was upgraded to handle 2" wafers.

* A double layer Si_3N_4/SiO_2 antireflection coating which enhances response over the 0.5 - 1.7 um range was developed.

* A method for anisotropic, precisely controlled CH_4/H_2 plasma etching for enhancement of response at short wavelengths was developed.

* Electronic and optical testing methods were developed to allow full characterization of detectors with novel size and spectral response characteristics.

On the basis of the work and results achieved in this program, we conclude that large size, high shunt resistance, high quantum efficiency InGaAs pin detectors are not only feasible but also manufacturable on industrial scale. This novel device spans a significant portion of visible and near infrared spectral range and it will allow a single detector to be used for the 0.5 - 1.7 um spectral region, rather than the presently used silicon (for 0.5 - 1.1 um) and germanium (0.8 - 1.7 um).

Table of Contents

I. Introduction

In this report we describe the development and production of a 5 mm active diameter InGaAs photodetector, operating in the 0.5 - 1.7 um wavelength range. Both the size and the operating range are new and unique features which make these devices attractive for a variety of applications.

The detection and measurement of electromagnetic radiation in the 0.3 - 2.0 um wavelength range is important in many areas of science and technology. This wavelength range spans ultraviolet (UV), visible (VIS) and near-infrared (NIR) portions of the spectrum, and just the detection and measurement of the visible light has innumerable uses, e.g. from photo cells regulating the opening and closing of elevator doors to sophisticated charge coupled devices (CCD) used in low light television mini cameras. Among the many other applications are UV, VIS and NIR spectroscopy, detection of light of the most popular lasers (e.g. He-Ne, ruby, Nd: YAG), applications in fiber optic networks operating at 0.82, 1.30 or 1.55 um, etc.

The most widely used devices for the above purposes are silicon photodetectors. Silicon detectors have high quantum efficiency, excellent signal to noise ratio, are very fast and reliable, and quite cheap as well. Utilizing silicon IC technology, it is relatively simple to integrate silicon detectors with other active components or to produce linear or 2-dimensional arrays with a large number of detector elements. In fact, the only drawback that silicon has is the inability to detect past 1.1 um, as determined by its bandgap of 1.12 eV. The next group IV semiconductor is germanium with a bandgap of 0.66 eV, and thus capable of detection in the range of 0.9 to 1.8 um. However, germanium is a much poorer detector than silicon. Its quantum efficiency is lower, its signal to noise ratio worse by several orders of magnitude, its speed of operation and reliability also worse, and the ability to produce integrated structures is quite limited.

EPITAXX, Inc. produces detectors based on InP/InGaAs epitaxial layers. These detectors approach silicon in terms of quantum efficiency, signal to noise ratios and the speed and reliability of operation. Their usual detection range is 0.9 - 1.7 um. In this report, we describe the development and production of InGaAs detectors capable of operating in the 0.5 - 1.7 um range with satisfactory performance characteristics, or in other words, a silicon- like detector capable of covering most of the visible and NIR spectral range.

InGaAs detectors have been widely used in fiber optic telecommunication networks for quite some time now[1]. The small size of the fiber and the requirement of fast operation (up to 1 GHz or higher) dictated that InGaAs detectors be quite small in size, typically 50 - 150 um in diameter. There are, however, other applications for InGaAs detectors, notably in optical power meters, spectrometers and other instruments where larger size detectors are required. For this reason, EPITAXX, Inc. has developed and successfully marketed InGaAs detectors 0.5, 1, 2 and 3 mm in diameter, operating in the 0.9 - 1.7 um range[2]. In this report, we present the newly developed 5 mm diameter detector and describe its performance characteristics.

II. State of the art of InGaAs detectors

In this section, we shall briefly review the state of the art of large diameter (i.e. 0.5 - 3 mm) InGaAs photodetectors produced by EPITAXX, Inc.

a) Structure of the detector

Figure 1a shows a structure of a pin detector manufactured by EPITAXX, Inc. Figure 1b is a SEM micrograph of epitaxial layers in a typical pin structure. The substrate is n^+ doped InP. The basic substrate issues are defect concentration, usually expressed as the etch pit density (EPD), quality of the surface finish, i.e. absence of large concentration of defects and slip lines toward the edge of the wafer because this influences the morphology of epitaxial layers and uniformity (variation of thickness and indium composition over the wafer). There are 3 epitaxial layers grown on the substrate. The first is the InP buffer layer, 1-3 um thick, usually undoped. The role of this layer is to make a transition from the substrate so that some of the substrate defects and imperfections do not propagate into the $In_{0.53}Ga_{0.47}As$ absorption layer, which is the second epitaxial layer. The basic requirements of the absorption layer are sufficient thickness (> 2 um) to assure complete absorption of incoming photons, lattice matched composition for adequate electronic properties and low doping (< 5×10^{15} carriers/cm^3) for low capacitance and leakage current. The third epitaxial layer is the InP cap layer. Since the InP bandgap is 1.35 eV (vs. 0.71 eV for $In_{0.53}Ga_{0.47}As$), both the surface leakage currents and surface recombination of photogenerated carriers are reduced. This enhances the noise performance thus increasing overall quantum efficiency by 20 - 30%. The thickness of the InP cap is usually about 1 um and thus the cap cuts off wavelengths below 0.91 eV where InP absorbs. For the purpose of the present program (i.e. response to 0.5 um) the cap thickness was reduced. The very top layer is a plasma deposited Si_3N_4 dielectric coating, which provides passivation, or in other words, assures the reliability of the device. Among the most important properties of the dielectric coating are a low concentration of surface states at the InP/Si_3N_4 interface in order to reduce surface leakage currents.

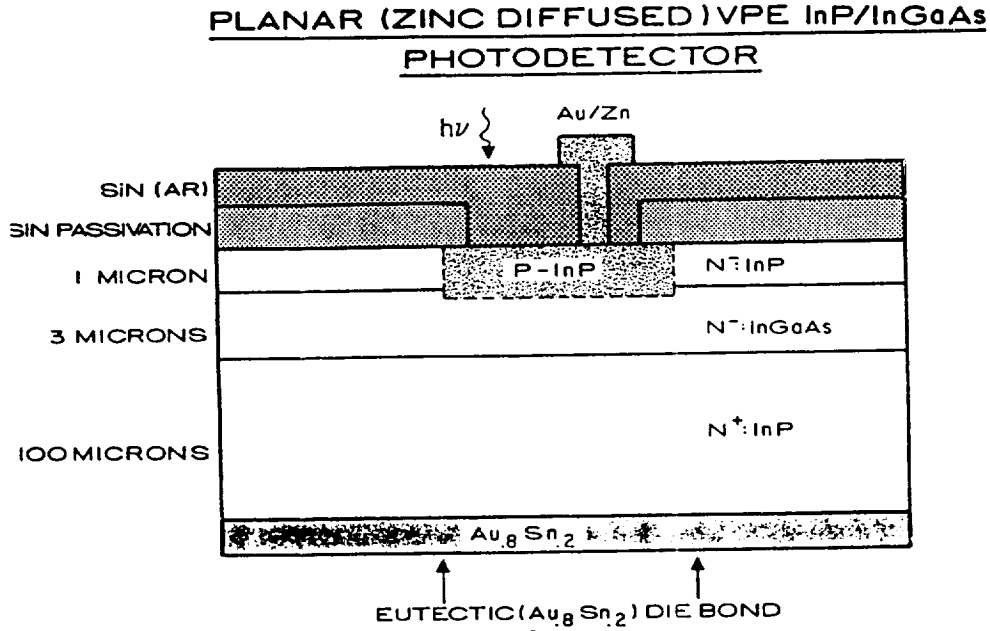

Figure 1a. Layer structure of a typical pin detector.

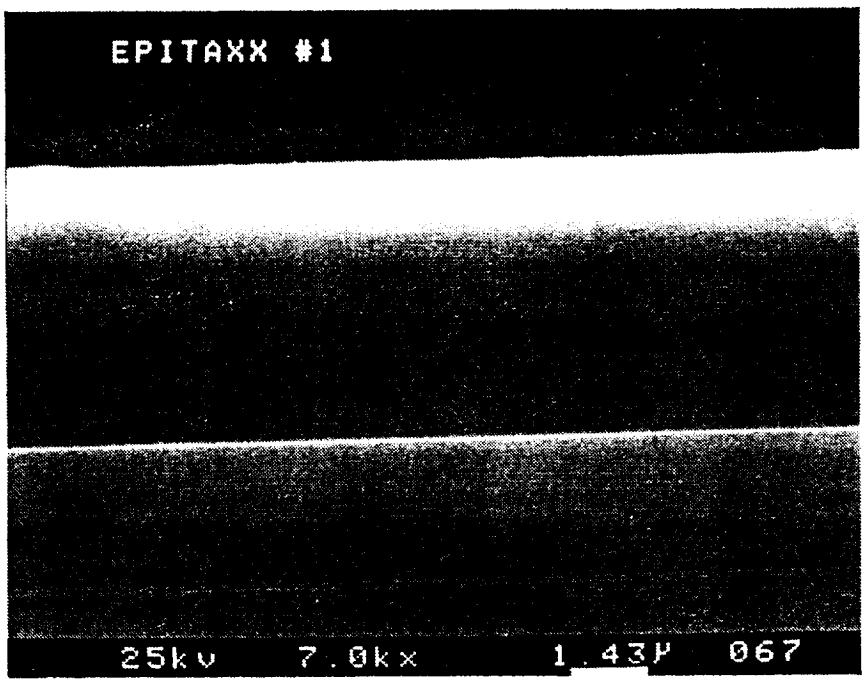

Figure 1b. SEM micrograph of epitaxial layers in pin detector.

The other role of Si_3N_4 is to serve as an antireflection coating to enhance the responsivity of the detector.

Finally, there are p-side contacts (AuZn alloy) and n-side contacts (AuSn alloy) to provide low resistance, ohmic contacts to the device.

b) Spectral response

Figure 2 shows the plot of the responsivity of InGaAs photodetectors. The cut off wavelength of 1.7 um is determined by the 0.71 eV band gap of the lattice matched $In_{0.53}Ga_{0.47}As$ absorption layer. On the short wavelength end the responsivity is reduced by the InP cap layer (band gap 1.31 eV) which absorbs light shorter than 0.91 um. Thus, at 0.8 um the responsivity is typically 0.1 - 0.2 A/W, which is considerably less than the values of 0.7 - 0.9 A/W observed in the 0.9 - 1.7 um range.

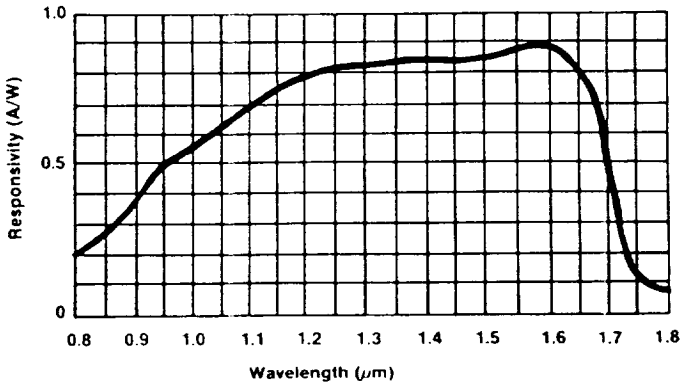

Figure 2. Responsivity of typical InGaAs detectors.

c) Shunt resistance (R_{sh}) and noise

The shunt resistance is the slope of the I-V characteristic curve across the zero bias region. In Table 1, it is calculated as 5 mV/I_d (at 5 mV). This parameter is related to the detector noise (i_j) by:

$$i_j = (4kTB/R_{sh})$$

(B = equivalent noise bandwidth (Hz))

The above equation assumes that only Johnson noise is generated by the shunt resistance and that there is no dark current. The shunt resistance is therefore a good indication of the noise generated by the photodiode in the absence of voltage bias.

The lower limit of light detection is expressed as the amount of incident light needed to obtain a signal to noise ratio of 1. It is given by the NEP (Noise Equivalent Power):

$$NEP = i_j/R \quad (W/Hz^{1/2})$$

where R is the peak responsivity of the photodiode.

Table 1 lists the typical shunt resistance and NEP of EPITAXX InGaAs photodetectors from 0.5 to 3.0 millimeters in diameter.

Table 1. Typical Shunt Resistance at 25°C

Parameter	Diameter (mm)				Units
	0.5	1.0	2.0	3.0	
R_{sh}	20	5	1	.5	Mohm
NEP @ 1.6 um	.01	.2	.3	.5	$pW/(Hz)^{1/2}$
$D^* = A^{1/2}/NEP$		1.6×10^{12}			cm $Hz^{1/2}/W$

The detectivity D*, which is inversely proportional to NEP, is above 10^{12}cm $Hz^{1/2}/W$, which is similar to values for silicon.

d) Speed of response

The speed of response of the detector, or its rise time and fall time, is expressed as:

$$t_r = 2.2\ R_t C$$

where R_t is the sum of the load and series resistances and C is the total package capacitance. For InGaAs photodiodes, the series resistance is typically 20 Ohms.

Table 2 shows typical rise time values for 0.5 to 3.0 mm diameter devices with a 50 Ohm load.

Table 2. Speed of response

Active Diameter (mm)	Capacitance (pF)	Voltage bias (V)	Rise/Fall time (nS)
0.5	20	-5	1.5
1.0	100	-1	15
2.0	600	0	100
3.0	1000	0	150

e) Effects of temperature

InGaAs detectors are capable of operating in the temperature range from 77K to 400K. An increase in temperature has two major effects: i) it increases the cutoff wavelength by about 9A per degree (at 250K the cutoff is about 1.65 um, at 350K, it is about 1.75 um); and ii) it increases the noise (or decreases the shunt resistance).

Figures 3 and 4 illustrate the effects of temperature on cutoff wavelength and shunt resistance, respectively.

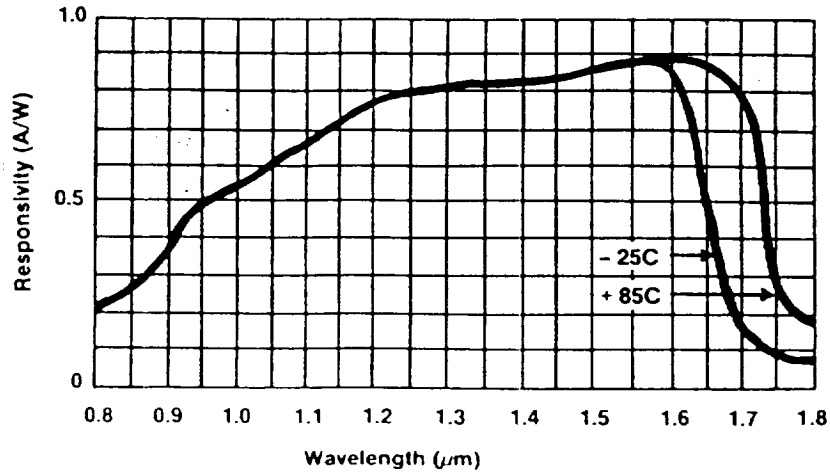

Figure 3. Effect of temperature on the cut-off edge of InGaAs detectors.

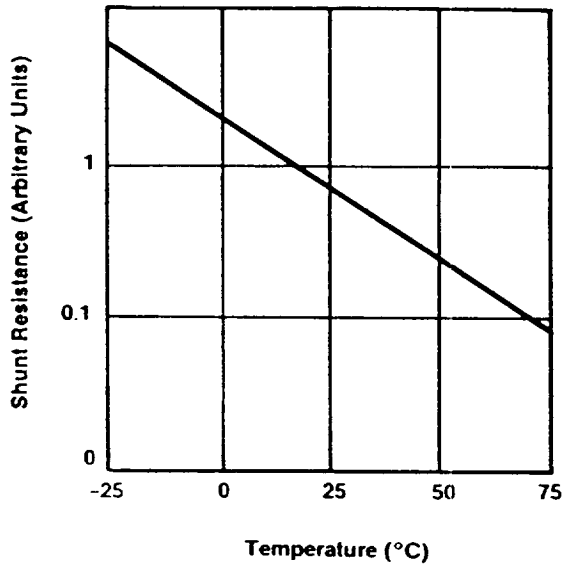

Figure 4. Effect of temperature on shunt resistance of InGaAs detectors.

III. Goals of the present program

We shall recapitulate the goals set out at the start of this program.

We proposed to develop a unique laboratory standard indium gallium arsenide 5 mm active diameter detector which has high QE over the 0.5 to 1.7 nm spectral range.

A number of fundamental technical problems must be solved before a reproducible laboratory standard type detector could be mass produced economically (i.e. at a cost somewhere between present-day silicon and germanium detectors). These problems include:

- o the ability to produce large wafers with uniform epitaxial layer thicknesses
- o the ability to reproducibly make low resistance (< 100 ohm) ring contacts to 5 mm detectors
- o the ability to make 5 mm diameter InGaAs detectors with shunt resistances which are consistently at or above 15,000 ohms
- o the ability to make InGaAs detectors whose quantum efficiency is at or above 50% over the 0.5 - 1.7 nm spectral range

In order to solve these problems and to prepare for the Phase III production program, EPITAXX proposed a development effort consisting of the following tasks:

- o Construct and optimize a VPE reactor for the growth of uniform, high quality InP/InGaAs epitaxial layers on large diameter indium phosphide substrates to produce 5 mm detectors economically.
- o Optimize a new process for large area visible InGaAs detector fabrication where zinc diffusion and metal contacts are applied onto a thick (1 micron) InP layer, which is then selectively removed in the active area of the detector to enhance the visible response.
- o Develop techniques to deposit multi-layer dielectric anti-reflection coatings onto InP with reflectivity below 5% over the 0.5 - 1.7 nm spectrum.
- o Develop zinc diffusion techniques to precisely position the p/n junction in InGaAs in order to optimize quantum efficiency at short wavelengths.
- o Optimize p-type (gold-zinc) ring metal contacts to InP on 5 mm diameter detectors which have reproducibly low resistance and good adhesion.
- o Operate devices at 125^{o}C and determine their reliability.

At the end of the program, EPITAXX proposed to deliver ten state-of-the-art devices to NASA. Performance goals for these 5 mm diameter devices were to include:

- near 100% internal quantum efficiency
- external quantum efficiency of 50% from 0.5 to 1.7 nm
- shunt resistance above 15,000 ohms at room temperature
- uniform response within ±5% across surface
- reliable operation at +125 degrees centigrade

In the following sections, we shall discuss various aspects of the developing program which led to the successful realization of all of the goals listed above.

IV. Epitaxial Deposition

a) Present VPE process and equipment

Vapor phase epitaxy (VPE) of III-V materials by the hydride method is a well established method which has been successfully used for the growth of InGaAs detectors and InGaAsP emitters used in fiber optic systems. The double barrel reactor (Figure 5) is a particularly convenient embodiment of this method because it facilitates growth of multilayer heterostructures, such as those employed in detectors and emitters (3).

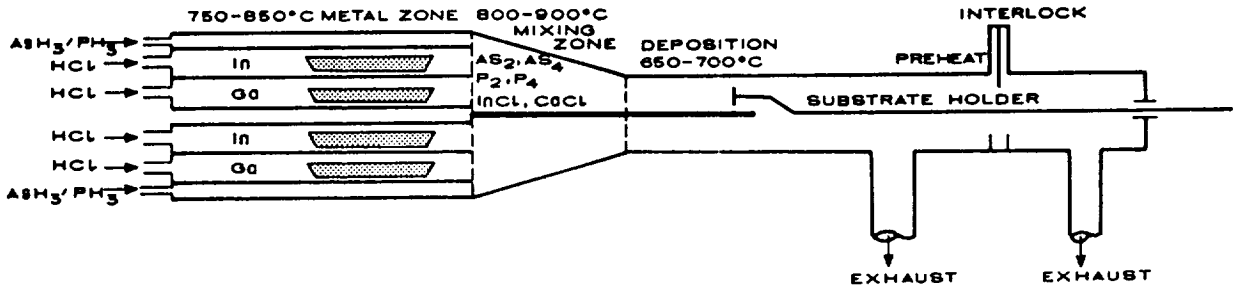

Figure 5. Schematic representation of the hydride VPE reactor.

The thermodynamics of the system and the effects of temperature, flow ratios and input concentration on growth and composition of InGaAs alloys has been discussed in some detail (4). The transport phenomena, e.g. momentum, heat and mass transport in hot wall reactors have not been completely understood, as opposed to cold wall silicon reactors, where these studies have been carried out. Difficulties arise because hydride reactors, due to the short growth zone and the substrate holder arrangement, encounter the so-called entry effects of the fluid flow, where transport phenomena are ill-defined. Nevertheless, it is possible to give a qualitative discussion of the effects of transport phenomena on compositional and thickness uniformity of the grown layers. Figure 6 depicts flow phenomena in a hydride reactor growth zone for the case of a substrate oriented parallel to the flow.

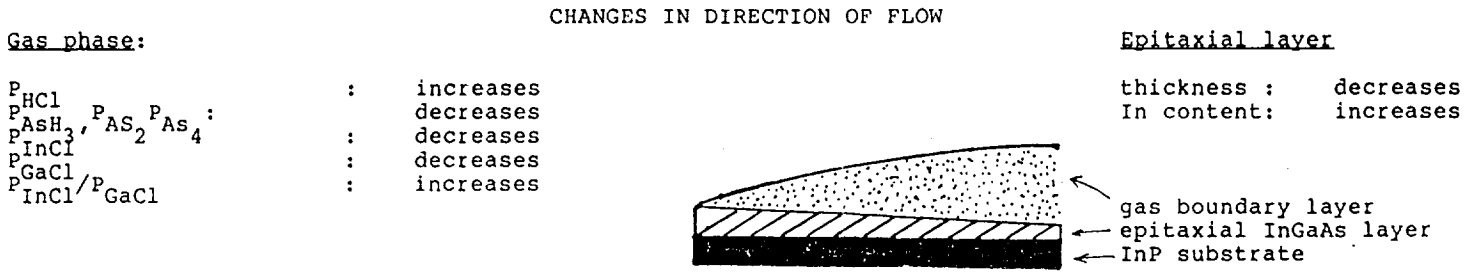

Figure 6. Fluid flow phenomena in hydride VPE.

There are several important points covering the thickness and compositional uniformity of $In_{.53}Ga_{.47}As$ layers grown in orientation parallel to the flow:

a) Only a very small fraction (~0.5%) of introduced reactants end up in the epitaxial layer. Most of the deposition occurs downstream from the substrate in the exhaust of the reactor.

b) Only those species in the immediate vicinity of the substrate participate in the deposition reaction; there is a gas boundary layer of about 1 mm in thickness from which reactants are supplied to the growth interface.

c) The (PInCl/PGaCl) ratio, which is initially 10, increases in direction of flow because, for the deposition of $In_{0.53}Ga_{0.47}As$, approximately equal number of both metal atoms must be deposited from the vapor phase, and the less abundant Ga atoms are relatively more affected.

d) The consequence of increasing the InCl/GaCl ratio is the increased In content in the downstream portion of the wafer. Increases from 53% to 55% In have been experimentally observed.

e) The thickness decreases in the direction of flow due to the depletion of reactants; experimentally we observed thickness variation up to 30% over 3 cm.

The thickness and composition non-uniformities become particularly troublesome in the case of large detectors, where these nonuniformities might manifest themselves across the large (i.e. 5 mm dia.) device itself and not only across the wafer. The economics of producing large area devices also presents a problem. The present reactors usually produce one wafer of 1-2 sq. inches per run. Assuming normal yields, this wafer might give well over a thousand small devices (e.g. 75 mm dia.) but only 10 or less 5 mm dia. detectors. Thus, both the reactor technical performance and its capacity require significant improvements if the objectives of producing high quality devices economically are to be met. These improvements are the topic of the next section.

b) New reactor design

In order to satisfy more stringent criteria for the uniformity of epitaxial layers, we designed and built a new hydride VPE reactor system capable of handling 2" diameter and larger substrate wafers. This reactor system consists of several subsystems, which are described next.

i) Gas Cabinets

Gas cabinets are designed for a continuous flow of air to be pulled thru the system by end exhaust blower for venting of reactive gases in the event of an accidental leaks.

ii) VPE Epitaxial Gas Control System

Mass Flow Controllers - Twenty-six (26) stainless steel, Tylan Model 280 mass flow controllers, calibrated for the appropriate gases, are provided for monitoring and controlling each of the reactor gas lines. Actual gas flows are digitally displayed on the electrical control panel in direct units of flow. Ten turn digital readout set points are provided for setting each mass flow controller.

Gas Valves - Nineteen (19) NUPRO air-operated stainless steel BN series bellows valves with VCR connections and sequenced by 24 volt D.C. electric solenoids are provided for sequencing of all gas porting functions.

Seats and O-Rings - Only Viton, Teflon and Kel-F materials are used on seats that come in contact with the gas stream. All O-Ring seals are Viton.

Lines and Fittings - are 316L stainless steel (16 RMS or better interior finish) and automatic Heliarc butt-welded (inert gas welded to eliminate oxide contamination) wherever practical. Prior to final assembly, the tubing was cleaned and passivated to eliminate any possible contaminants. Valves and mass flow controllers are connected by Cajon VCR fittings to allow for easy removal during system maintenance. Upon completion, the system was Helium leak checked to a level of 5×10^{-9} Atm cc/sec, and Hydrogen leak checked to 50 PSI with no detectable leak.

Electrical Control System - is supplied with manual controls for sequencing of all system functions. A Tylan Tymer 16 is provided for sequencing valve functions. Indicator lights sequence on with system function in both the manual and automatic control mode are provided to assist in system operation. A silk-screened graphic gas flow schematic is provided on the front control panel for easy observation of all reactor functions.

iii) VPE Epitaxial Growth Furnace

Heating System - a low mass six zone resistance heated horizontal clamshell furnace operating at temperatures up to 1000 degrees Celsius is provided. Temperature control is accomplished by the continuous proportioned output of the Eurotherm temperature controller, a Type "R" thermocouple and SCR power pack, provided for each heated zone. Each Eurotherm controller has a built-in deviation alarm, PID self tuning and adaptive tuning capability, and thermocouple failure protection. Power to the heating element is via zero angle fired thyristors, which result in no overall distortion on the incoming power lines.

Profiling Thermocouples - Ten (10) additional type "R" thermocouples are provided within the heating element for monitoring and profiling the heated zones. The thermocouples are connected thru a switch to a digital readout to display temperature readings.

Reaction Chamber Cabinet (Hood) - is designed to have a continuous flow of air pulled thru the Reaction Chamber into an exhaust blower. The constant negative pressure minimizes the possibility of an accidental leak outside the equipment. A flow switch is incorporated within the reactor exhaust to ensure proper exhaust flow during system operation.

iv) Reactor Tube - Version 1

The reactor tube for the new system differed significantly from the standard tubes in the two older EPITAXX reactors. The most obvious difference was the size of the tube. Its over all length was 78" vs. 71" for standard tubes. The larger overall length allowed longer metal boat zones so that larger quantities of indium and gallium could be placed into the reactor. Thus, the reactor can be operated for a longer period of time between refills of the metal boats. The deposition zone was also several inches longer. The purpose of this change was to improve gas flow patterns for better uniformity of the epitaxial layers. Furthermore, a longer deposition zone could possibly accommodate more than one wafer per run.

There were also several changes in the geometry of the reactor. The tubes containing indium boats were rectangular, rather than the standard round shape. The reason for this change was to enhance the conversion of the HCl into InCl by reducing the head space over indium boats.

The mixing zone geometry of the standard tubes was retained because it provides satisfactory mixing of reactants. The deposition zones were made of 4" X 1" rectangular tubes, stacked one above the other. These are much larger than the standard deposition zone which is 1/2 of the 53 mm ID round tube. The rectangular tube could easily accommodate 2" or 3" wafers. Furthermore, in analogy with silicon epitaxial reactors, it was expected that the rectangular shape will lead to better uniformity of the deposited layers. This is due to the fact that in rectangular tubes, the distance between the wafer and the roof of the tube is equal for all parts of the wafer. In round tubes, the edges of the wafer are closer to the roof. This means that the gas flow velocities and thus the reactant transport phenomena are not uniform across the whole wafer. This usually leads to non-uniform epitaxial growth.

The downstream portion of the tube was also significantly larger than the standard tube (100 mm ID vs. 53 mm ID) to allow the easy insertion of longer wafers. Other components, e.g. the gate valve, the forechamber, and flanges, etc. were scaled up accordingly.

This tube (i.e. Version 1) is shown in Figure 7.

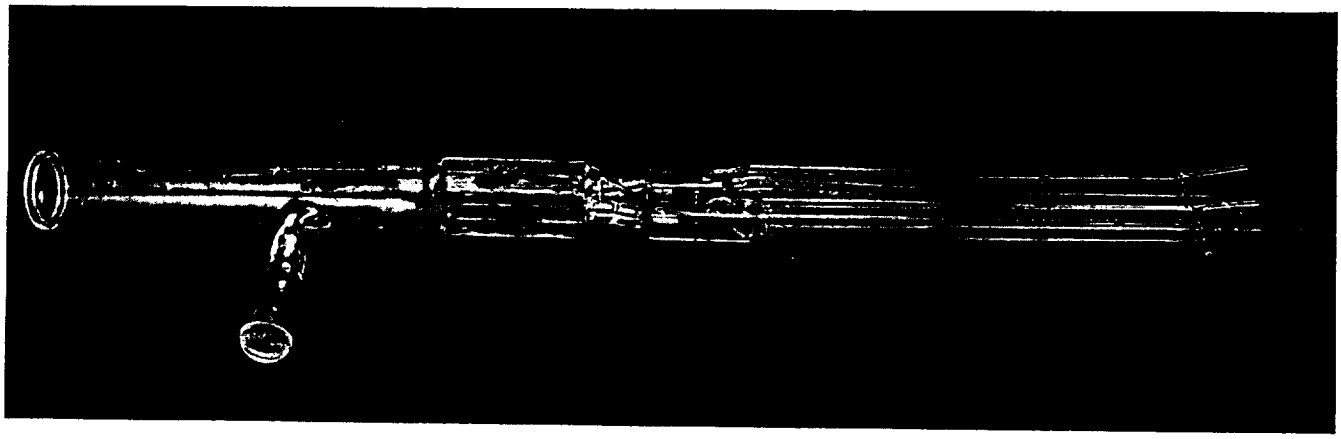

Figure 7. Reactor tube - Version 1.

v) Reactor Tube - Version 2

The tube just described (Version 1) represented quite a radical departure from the standard reactor tubes, both in the size and the geometry of crucial parts. The second version was designed with the idea to minimize differences with standard tubes, while still fulfilling one of the basic requirements of these programs, i.e. to achieve satisfactory deposition of InP and InGaAs epitaxial layers on a 2" diameter InP substrate.

The Version 2 tube was also 78" long overall. The indium boat tubes were round but longer than the standard and thus capable of larger indium loads. The mixing zone was the same as in standard tubes. The deposition zone was 1/2 of a 63 mm ID round tube. This means essentially the same geometry as the standard tube, yet capable of accommodating 2" diameter wafer.

The downstream portion was also 63 mm ID. Thus the Version 2 tube is just a slightly larger standard tube. However, this tube offers the possibility of achieving uniform growth by changing parameters such as carrier gas flow volume, partial pressures of reactants, various types of wafer holders, etc. This tube is shown in Figure 7b.

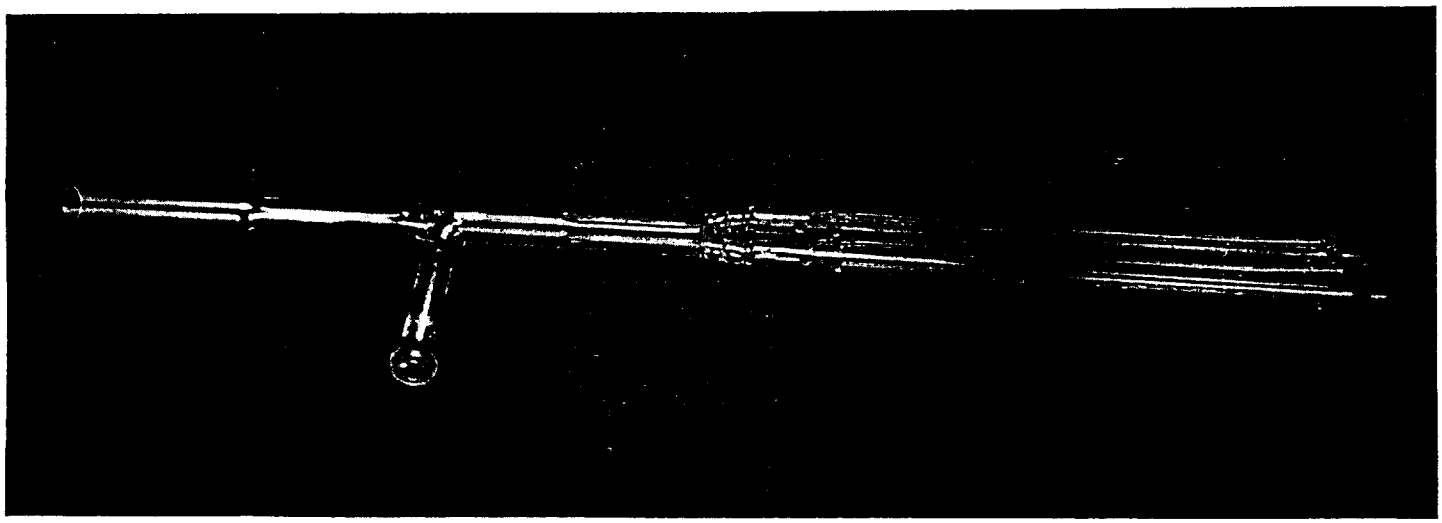

Figure 7b. Reactor tube - Version 2.

Figure 7c represents the external view of the new reactor built for the present program, showing the furnace, flow control panel, temperature controllers, gate valve, reactor cabinet, etc.

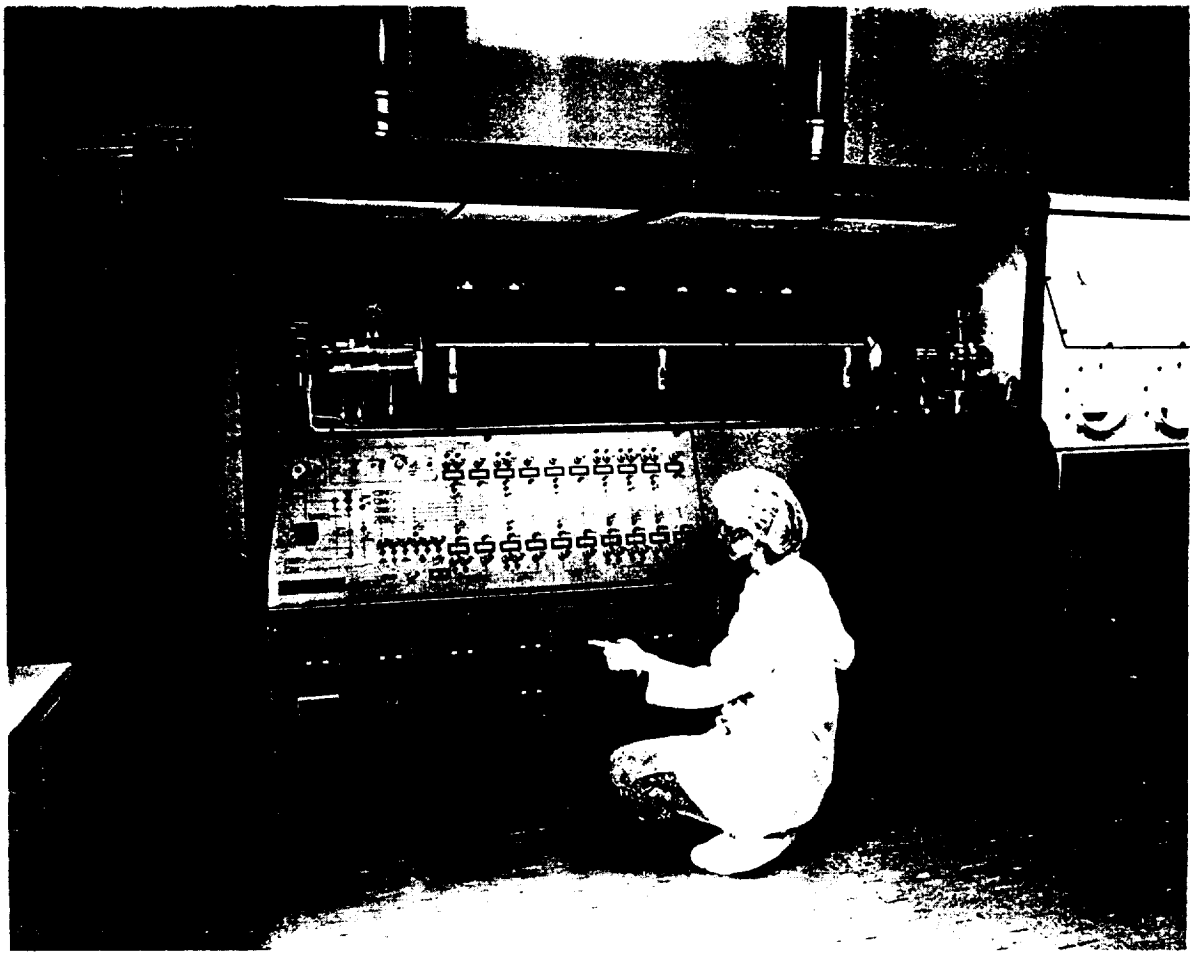

Figure 7c. External view of a new hydride VPE reactor capable of growth on 2" substrates.

vi) Reactor Tube - Version 3

A final version of the quartz reactor tube - based on lessons learned from the first two versions - gave the best results of the program. The major modification was a reduction of the preheat zone diameter down to the conventional 2 1/2" size used in our production reactors and the elimination of the "preheated" PH_3 line (used to prevent decomposition of the InP substrate wafer during preheat) used in version 2 (but not version 1). We also lengthened the preheat furnace in order to flatten the preheat temperature profile and to reduce entry effects which had degraded surface morphology. All in all, version 3 is quite similar to our standard production quartz tube except for a rectangular growth zone geometry and a slightly larger (2 1/2" diameter) size to accommodate a 2" wafer.

c) Optimization of epitaxial growth

Once the reactor system was installed and accepted from the manufacturer, we initiated a program to ascertain parameters for the optimal epitaxial growth. Since the size and the geometry of the new reactor differed significantly from standard reactors, it was not reasonable to expect that the growth conditions would be identical. We thus searched over a fairly wide range of experimental conditions.

Effect of flow velocity over In boats

Growth of InP was optimized first. The importance of the conversion of the HCl into InCl was already mentioned. This conversion occurs according to the following chemical equation:

$$HCl_{(g)} + In_{(l)} \text{ ---> } XInCl_{(g)} + (1 - X)\, HCl_{(g)} + X/2\, H_{2(g)} \quad (1)$$

X denotes the fraction of the HCl converted into InCl,
(1-X) denotes the fraction HCl remaining unconverted.

According to chemical thermodynamics at $T > 800^0C$, practically all (> 99%) HCl should be converted into InCl. In practice, it has been observed that the conversion amount depends on factors such as reactor geometry and the nature and velocity of flow of the HCl/H_2 mixtures over the In boats.

Figure 8a illustrates the effect of the flow of carrier gas (H_2) on the growth rate of InP. As one can see, there is a significant drop in the growth rate at higher carrier gas flows. We interpret this drop as a consequence of lower conversion of HCl into InCl. The unreacted HCl is swept into the deposition zone, where it slows the growth rate of the InP layers. Similar effects have been seen in growths of InGaAs and InGaAsP alloys (5). In the above experiments, the flow of HCl was kept constant at 30 sccm, the flow of PH_3 at 300 sccm and the flow of hydrogen was 6 l/min. in addition to the carrier gas flow over the indium boats.

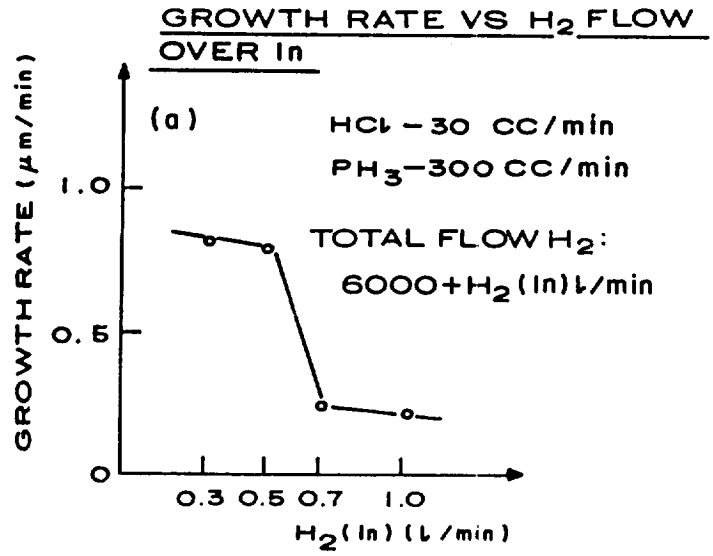

Figure 8a. Effect of the flow rate of H_2 over In boats on the growth rate of InP.

Effect of partial pressures of reactants

Figure 8b shows the increase of growth rate with increasing partial pressures of reactants, i.e. of input HCl and PH_3. The total flow of H_2 was maintained at 8 l/min. Since the flow velocity and consequently the nature of the flow and the thickness of the boundary layer depend primarily on the flow of the carrier gas (reactants are a small fraction of the total volume), the increase in growth rate with reactant partial pressures indicate that the growth rate is mass transport controlled. Higher reactant concentrations mean more reactants arriving at the growth interface per unit of time and thus the higher growth.

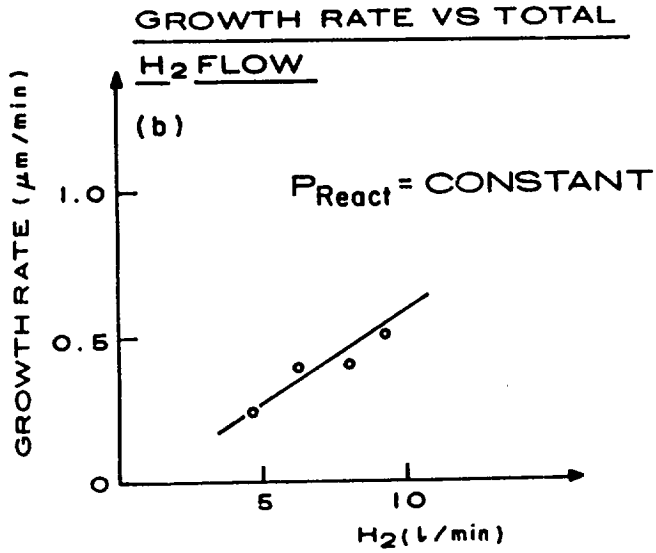

Figure 8b. Effect of the total flow rate of H_2 on the growth rate of InP.

Effect of carrier gas flow

Figure 8c shows that the growth rate increases with higher flows of H_2 carrier gas. The reactant flows were adjusted so that the partial pressures of reactants remained constant.

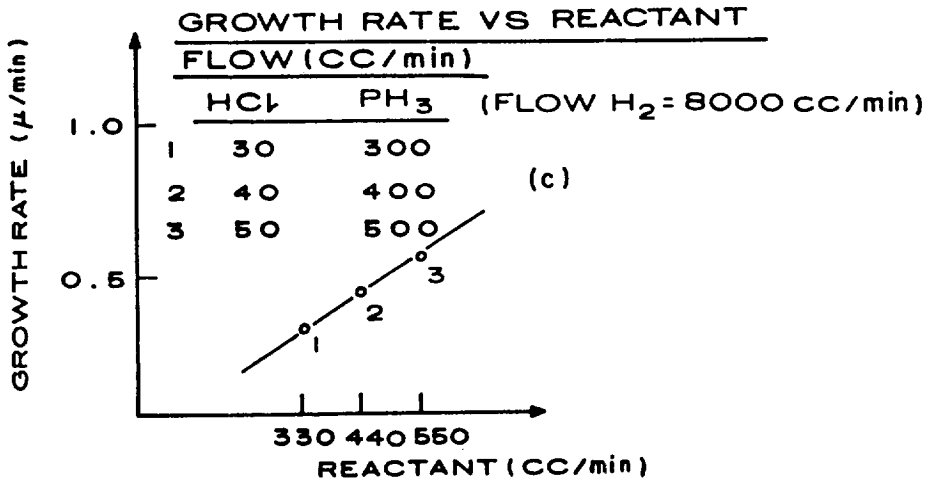

Figure 8c. Effect of partial pressure of reactants (HCl and PH_3) on the growth rate of InP.

The higher flows mean thinner boundary layers, which in turn mean higher transport rates to the growth interface. We thus again conclude that the growth rate is mass transport controlled. This means that the uniformity of deposited layers can be affected by the geometry of the reactor (e.g. by tilting the wafer holder to influence the thickness of the boundary layer, etc).

d) Results of optimization of epitaxial growth

As with all new reactors, numerous runs were needed to enable the growth process to produce the wafers specified by this program. The optimization of the growth rate was already described. Equally important is the morphology of grown layers, which is greatly influenced by many factors, e.g. growth temperatures, preheat temperature, substrate quality, wafer pregrowth preparation techniques, etc.

Figure 9 shows photographs of various areas of the pin wafer no. 10357 with different degrees of roughness resulting most likely from a non-uniform temperature in the preheat and growth zones. Figure 10 shows photoluminescence (PL) curves associated with these areas. Two things should be noticed - all PL curves peak at 1654 nm corresponding to a bandgap of 0.75 eV and signifying uniform composition in all areas measured. The other feature is that the intensity of PL decreases with increased roughness of the area measured. Curve X represents PL from a sample of known high quality epitaxial wafer. Better areas of wafer no. 10357 have PL intensities close to the control values indicating good quality of epitaxial growth.

Figure 9. Various degrees of surface roughness in different areas of wafer no. 10357.

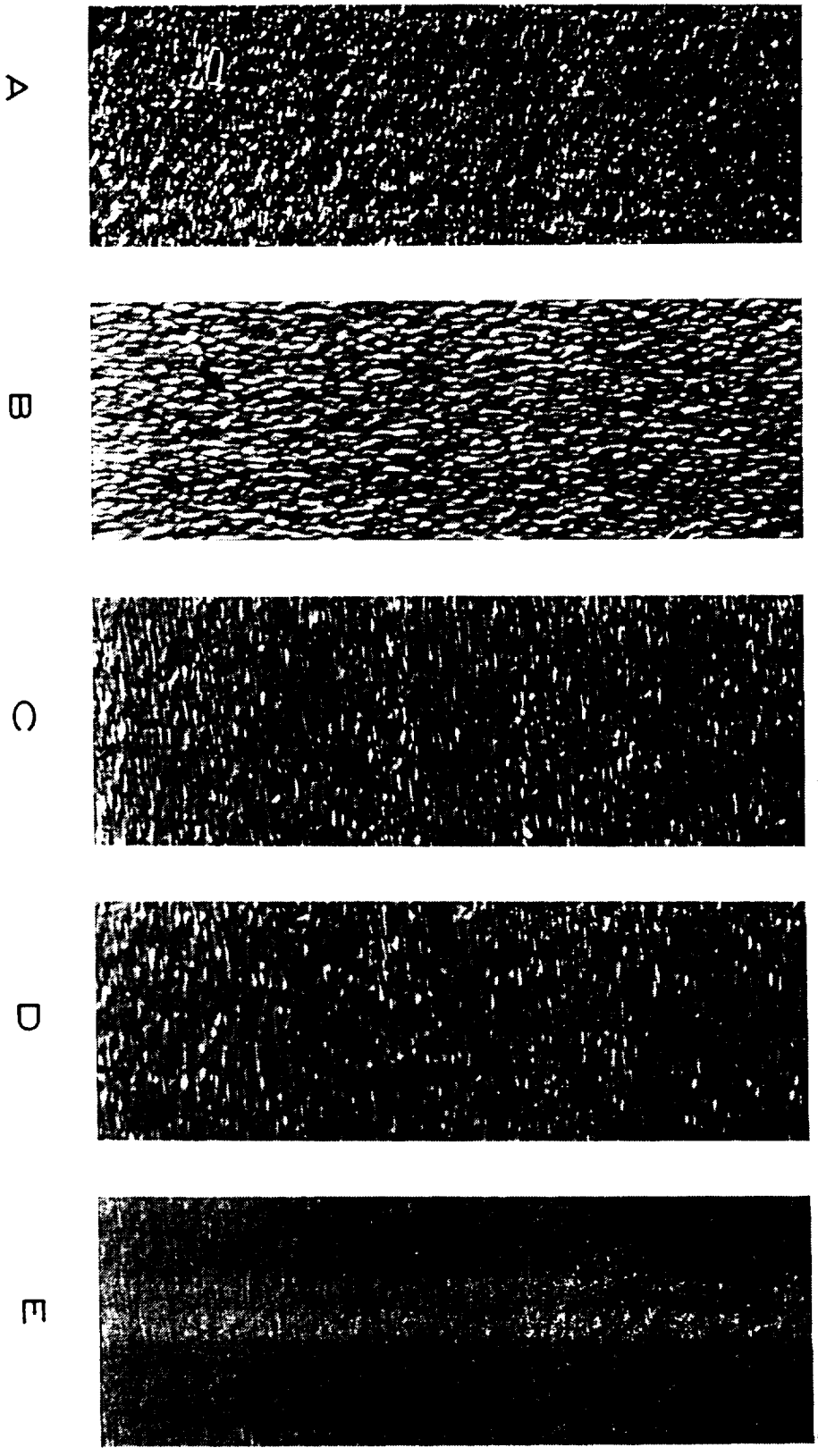

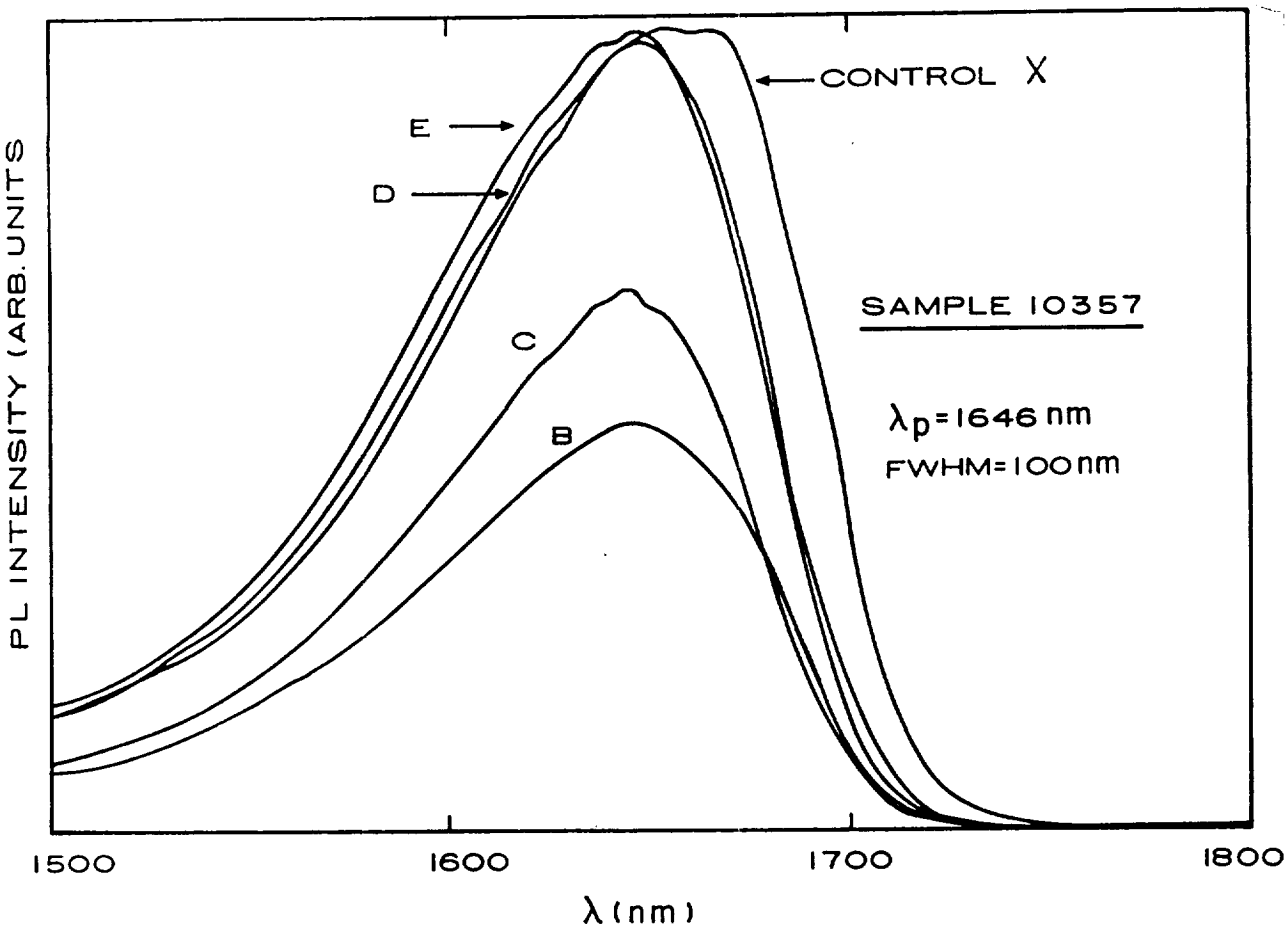

Figure 10. Photoluminescence intensity curves from areas with various degrees of roughness (the roughest area (A) gave no PL signal).

Figure 11 shows results of the CV analysis of wafer no. 10357. Curves A,B, and C denote thickness and doping levels of the InGaAs layer in the pin structure, taken at 3 different locations on the wafer. Again, one concludes that the thickness (1.7 - 2.0 um) and doping uniformity (3 - 4 X 10^{15} carriers/cm^3) are satisfactory.

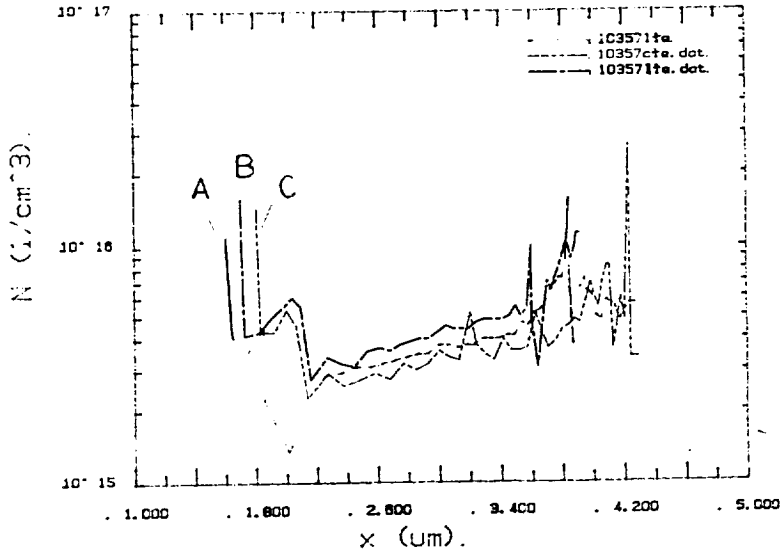

ORIGINAL PAGE IS
OF POOR QUALITY

Figure 11. Results of CV analysis of three different areas of wafer no. 10357 (curves A,B,C) showing thickness and doping of the InGaAs layer.

Approximately 300 growth runs were performed in the new reactor, the majority of those aimed at the optimization of various variables. At the same time, a significant number of runs of processable wafers were also made. The best results on 2" wafers obtained so far are as follows:

	Growth Rate um/min	Uniformity ± %	Background doping n-	Compositional uniformity (±% In)
InP	0.3 - 0.5	5	8×10^{14}	na
$In_{.53}Ga_{.47}As$	0.25 - 0.35	5	2×10^{15}	± 1.5

The above quantities are well within our internal production specifications for the p-i-n detector epitaxial wafers and wafers thus could be submitted to the device processing department.

Figure 12 shows results of thickness and compositional characterization of epitaxial layers grown on a 2" wafer.

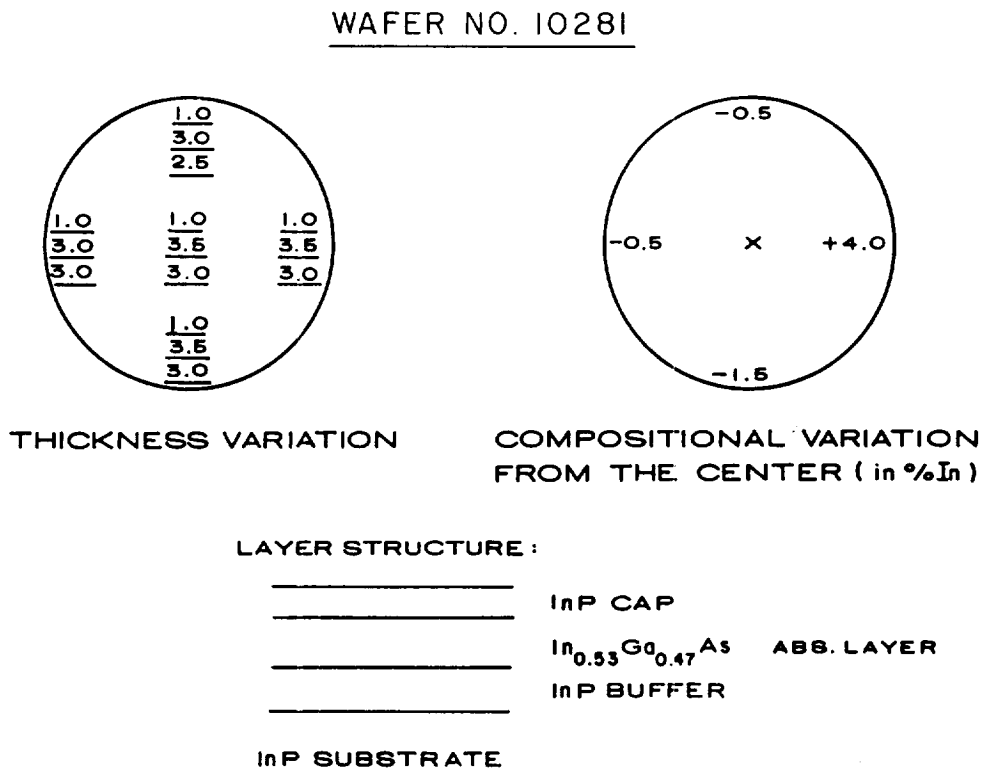

Figure 12. Results of analysis of thickness and compositional uniformity of epitaxial layers grown on 2" substrate.

Note: The thickness was determined by cleaving and staining the cleaved edge and then measuring with a metallographic microscope. The composition of the $In_{.53}Ga_{.47}As$ layers was ascertained by determining the lattice parameter by means of X-ray diffraction.

In addition to InP and InGaAs alloys, epitaxial layers of GaAs and InGaP alloys were also successfully grown in the reactor.

e) Conclusions and Recommendations About Reactor Tube Design

Much time, effort, and money was invested in the research and development of the quartz tube design during the course of this program. Details of the three versions used were described previously. The final "Version 3" actually produced four 2" diameter production quality $In_{.53}Ga_{.47}As$/InP pin detector wafers in a single afternoon. This could produce a total of 144 five mm chips or 800 three mm chips - all in a half-days' work! (typical out-the-door yields run about 40 - 50% for large area devices). Thus, this program has been extremely successful from the point of view of practical applications resulting from the R&D. Since much was learned about quartz tube design for hydride VPE reactors, we highlight the following conclusions and recommendations to be considered for future design work:

o It is better to develop a series of tubes with single changes, rather than one tube with several changes. Version 1 had many novel and radical changes from our standard, proven "production" tube in use at EPITAXX for over five years. Although occassional good growths occurred with the tube, it was basically "out of control" and since we had no real baseline to judge it by, we spent many months adjusting temperature profiles, preheat conditions, fluid profiles, etc. without being able to determine the main impediments to good growth.

Similarly, version 2, although closer in design to our production model, was sufficiently different that we were still unable to get consistently good results from it. We believe version 3 was successful (i.e. controllable and reproducible) because it was based on geometry which had already been proved at EPITAXX - except for a slightly larger growth zone that would accommodate 2" diameter wafers.

o When increasing size, scale all parameters up from models that already work. Thus, if cross-sectional tube area is increased 40%, increase all carrier and reactant flows by a similar amount. Length to width ratios and temperature profiles should also be held constant.

V. Processing of detectors

Figure 13 shows the structure of the detector capable of high responsivity in the 0.5 - 1.7 um range. There are several differences from the standard detector structure shown in Figure 1, the most obvious being the well etched in the active area of the detector. Etching thins the InP cap from 1 um in standard detectors to between 1000 and 2000A in the extended response detector. The transparency of InP for wavelengths below 0.91 um increases with decreasing thickness. At a wavelength of 0.88 um, a 1 um layer absorbs 73% of the incoming photons while a 1000A layer absorbs only 12%. The other important difference is the nature of the antireflective (AR) coating in the active areas. In the standard detector, the AR coating consists of 1 layer of Si_3N_4, optimized for minimum reflection at 1.3 um. In the extended response detector, the AR coating consists of a double layer of SiO_2 and Si_3N_4, adjusted for low antireflection in the whole 0.5 - 1.7 um range.

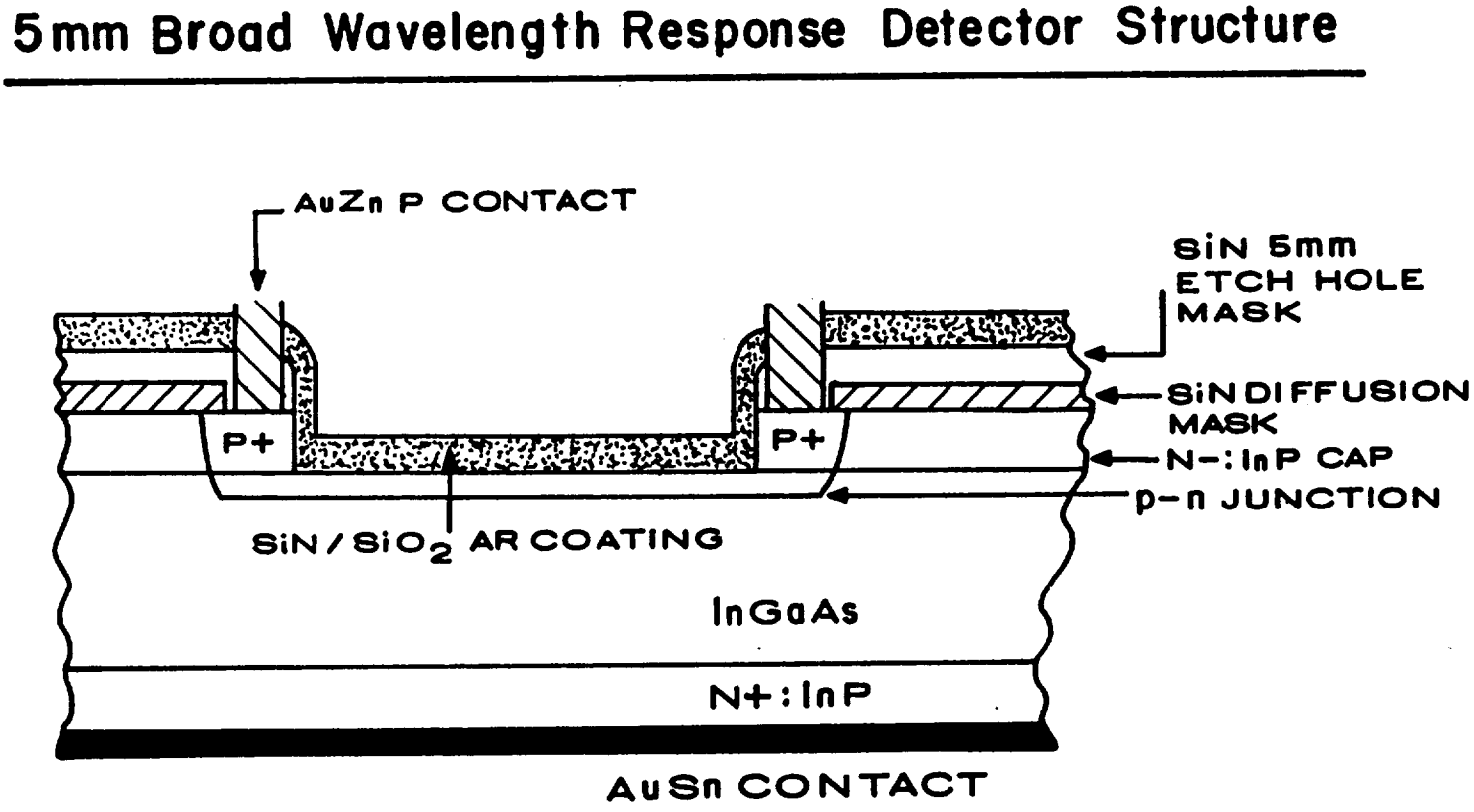

Figure 13. Structure of a detector with broad band response showing plasma etched well and a special antireflection coating.

We shall now describe the well etching and the AR coating deposition in some detail.

a) Well etching by CH_4/H_2 plasma

Well forming requires anisotropic etching and precise depth control. The anisotropy is necessary to ensure vertical side walls without under-cutting, so that subsequent layer of Si_3N_4 will form a continuous coating of the well. Precise control is needed to achieve proper depth of the well, i.e. to leave not more than 1000 - 2000A of InP to assure transparency, and thus a good responsivity at shorter wavelengths.

We applied a novel technique for dry etching of InP based on plasma etching with mixtures of methane (CH_4) and hydrogen (H_2). In comparison with the wet etching techniques or the older Cl_2 based plasma etching, this new process has significant advantages, e.g. it is anisotropic, it takes place at room temperature, and it seems to be capable of fine pattern definition, which is required for our purposes.

Plasma etching of semiconductors is a chemical reaction in which plasma activated gaseous species react with the solid semiconductor to form volatile reaction products, which are then pumped away.

Up to now, plasma-created active species was usually chlorine atoms, formed by the dissociation of Cl_2, CCl_4, $SiCl_4$ or some other chlorine containing gas. The overall reaction of plasma etching of InP with Cl_2 could be written as follows:

$$Cl_{2(g)} \xrightarrow{\text{plasma}} 2\,Cl_{(g)} \qquad (1)$$

$$6Cl_{(g)} + InP_{(s)} \xrightarrow{\text{heat}} InCl_{3(g)} + PCl_{3(g)} \qquad (2)$$

It is essential that the products of the etching reaction are volatile, so that they can be pumped away. This is not a problem for $PCl_{3(g)}$ which has a vapor pressure of 734 torr at 70°C. On the other hand, $InCl_{3(g)}$ has very low pressure at 70°C (~1 X 10^{-3} torr). Thus, in order to enhance the removal of $InCl_3$, etching must be carried out at temperatures over 300°C. This, of course, presents a problem, because at those temperatures, other materials, e.g. photoresists, dielectrics, metals, etc. are also attacked by chlorine.

Thus, the advent of the room temperature, anisotropic etching of InP and related compounds by the CH_4/H_2 mixtures is highly important. The process is very new and scarcely described in the literature (6,7). Very little is known about its mechanism. It is thought that some form of volatile metal organic compound is formed, which is easily pumped away, because it has reasonable partial pressure (> 100 torr), even at room temperature.

The etching process could be perhaps described as follows:

$$3CH_{4(g)} \xrightarrow{\text{plasma}} 3CH_{3(g)} + 1/5H_{2(g)}$$

$$3CH_{3(g)} + InP_{(s)} \dashrightarrow In(CH_3)_{3(g)} + PH_{3(g)}$$

This process amounts to be a reverse of the deposition of III-V compounds by the well-known metallorganic chemical deposition (MOCVD) method; i.e. methyl free radicals form the above products of the reaction. As far as we know, no detailed study of the mechanism of CH_4/H_2 etching has been reported. Also, little is known about the optimal process condition, needed to get the best etch rates, geometry control and surface quality.

In the course of this program, we had to determine processing parameters which would enable us to obtain pattern definition of better than 1 um in size and depth control to better than 0.1 um.

The following were found to be optimal conditions:

Flow rates

CH_4 - 10 sccm
H_2 - 40 sccm
Pressure = 40 mtorr
RF power = 180 watts
etch rate = 440A/min.

After every four minutes of etch time with CH_4/H_2, the wafers are back etched with O_2 plasma for two minutes to remove the carbon build-up deposited inside the chamber and on the portions of the wafer coated with SiN_x.

Figure 14 shows an InP ridge etched with CH_4/H_2 plasma at room temperature, clearly demonstrating the anisotropic nature of the process.

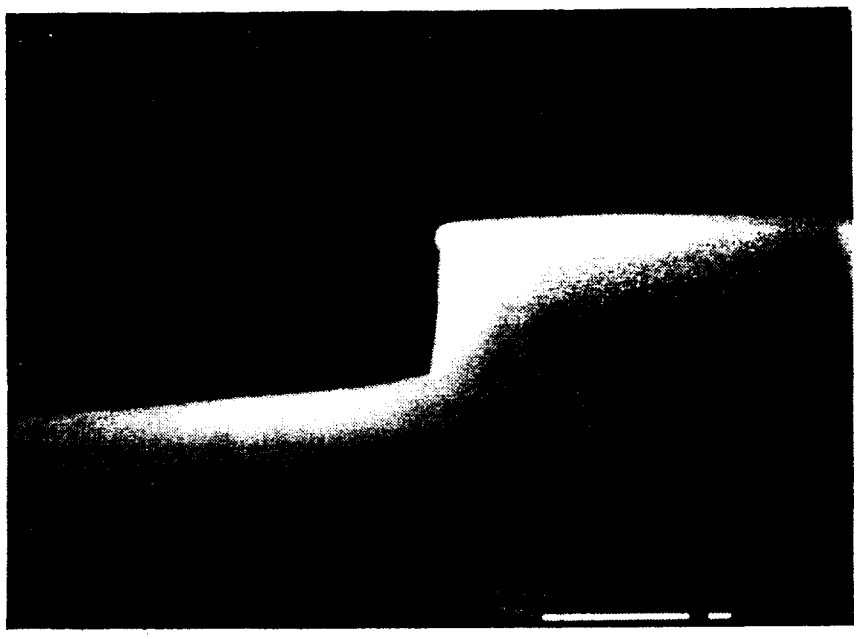

Figure 14. Vertical wall of the well etched by CH_4/H_2 plasma in InP (20,000X).

b) Deposition of Antireflection Coating

One of the main tasks of this program was to broaden the operating wavelength range (0.5 um to 1.7 um) of the antireflection coating. This was accomplished with a two film "high-low" dielectric stack deposited on the detector active area. This process had to be modified to allow silicon nitride (Si_3N_4) and silicon dioxide (SiO_2) sequential deposition onto the semiconductor. A starting point was the single layer, quarterwave thick, silicon nitride film deposited onto the InP cap layer via EPITAXX's PECVD (plasma enhanced chemical vapor deposition) system. This minimizes the Fresnel reflectance at a single wavelength; however, it doesn't have the wide operating spectral range required for this program.

The Fresnel reflectance is calculated for a single layer, silicon nitride film and a collimated input beam. Figure 15 illustrates the reflectance as a function of wavelength for a quarterwave film with a thickness optimized for 1.3 um. It also shows the Fresnel reflectance for an uncoated sample. This local minimum was chosen to accommodate the fiber optic transmission window which is at 1.3 um. The reflectance is asymmetric around the minimum, increasing faster at the shorter wavelengths than at the longer wavelengths. The Fresnel reflectance is less than 10 percent between 1 um and 1.7 um, and increases to maximum of 30 percent at 0.65 um. The reflectance is greater than 12 percent between 0.5 and 1.0 um. In order to reduce the reflectance, a single layer, quarterwave thick, must be expanded to multiple layers.

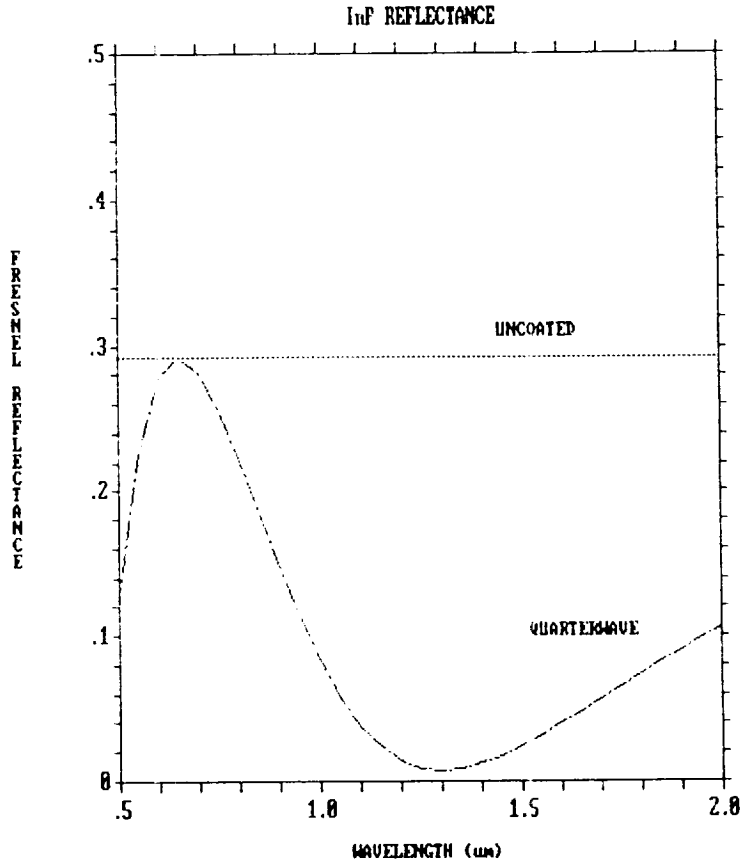

Figure 15. Fresnel reflectance for a single quarterwave antireflection coating optimized for 1.3 um. Also shown is Fresnel reflectance for an uncoated sample.

A two layer AR coating gives two Fresnel reflectance minima in the operating wavelength range. The starting point was to find two dielectric thin films that were compatible with EPITAXX's PECVD system. Since silicon nitride would form the first layer, the search was for the second material. Silicon dioxide has the necessary properties for the thin film stack. The predicted AR coating performance can be calculated for a two film stack without much difficulty (unlike for three or more layers). Figure 16 illustrates the calculated Fresnel reflection as a function of film quarterwave thickness for the light of 0.5 um and of 0.75 um. These calculations were performed by Prof. Angus McCloud of the University of Arizona Optical Sciences Center. Although these reflectance measurements are calculated, they are a good first order approximation for actual systems despite neglecting the wavelength dependence of the optical constants (especially at short wavelengths) which affect optical thickness. EPITAXX performed thin film (SiO_2 & Si_3N_4) growths using PECVD on Si substrate and on InP, and measured the reflectance between 0.5 um and 1.7 um for a collimated beam. Figure 17 shows results of experiment with an InP (n = 3.5 in the wavelenght range 0.5 to 1.0 um) substrate with a single 0.13 um Si_3N_4 layer. The thickness was monitored through its growth rate, and optically measured to obtain the required thickness. If the thickness was incorrect, the wafer was re-inserted into the chamber and made thicker, or the wafer was removed and its coating was "thinned" to have the proper thickness. Similarly, a 0.18 um SiO_2 layer was grown on the Si_3N_4 film. Figure 17 shows this system's reflectance between 0.6 um and 1.5 um. Also, a reference measurement for an uncoated sample is given. The reflectance is less than 10% between 0.725 um and 1.5 um.

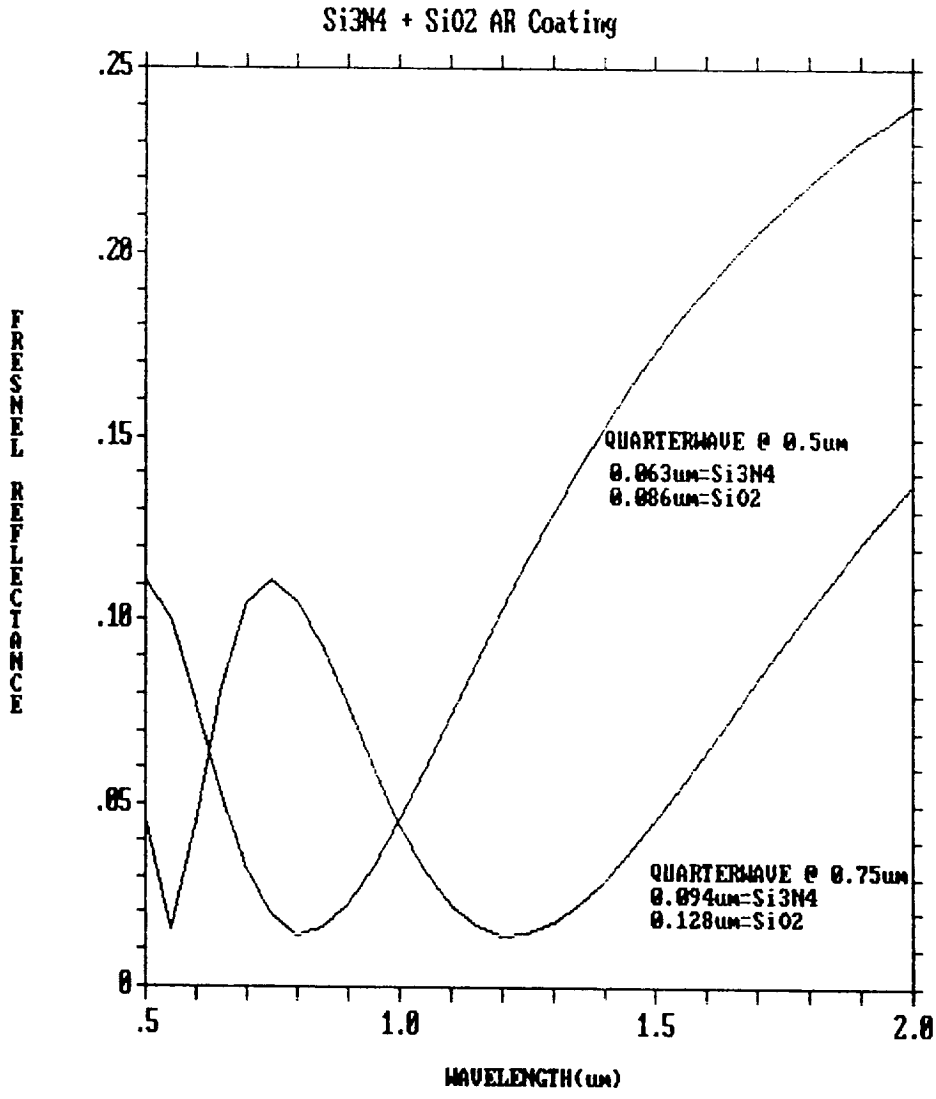

Figure 16. Calculated Fresnel reflectances for 2 layer Si_3N_4 + SiO_2 antireflection coatings for wavelengths of 0.5 um and 0.7 um (courtesy Prof. Angus McCloud - Univ. Arizona).

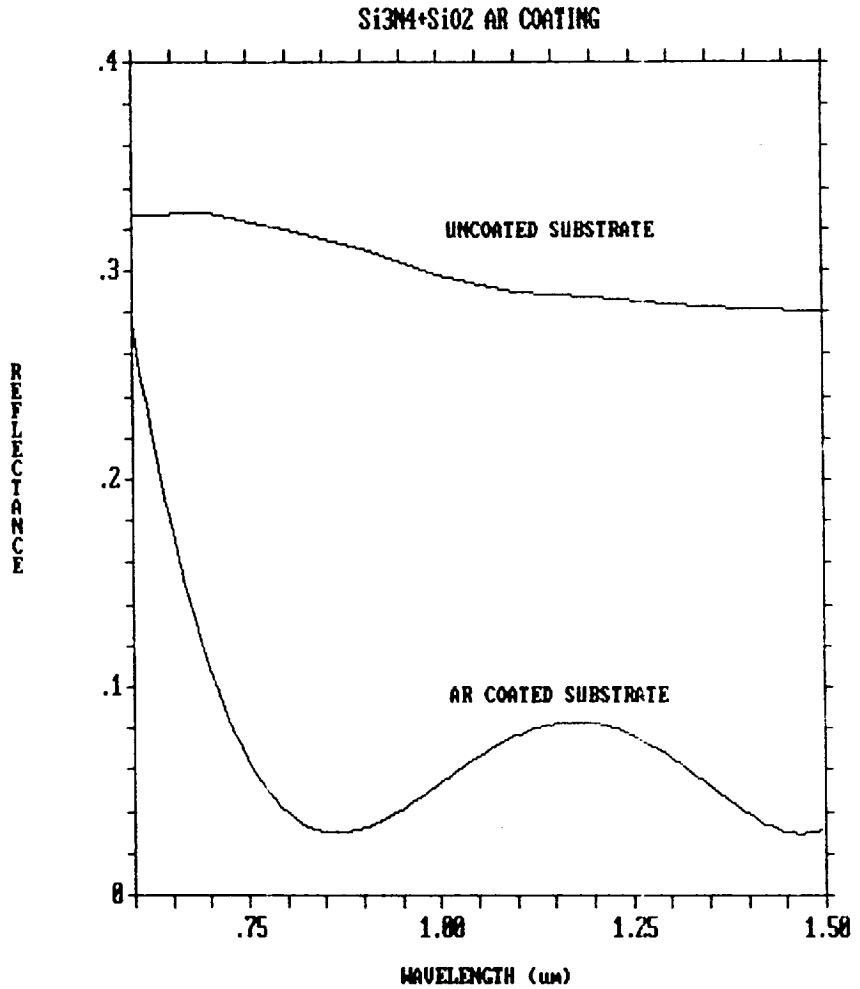

Figure 17. Fresnel reflectance of a 2 layer AR coating on InP; Fresnel reflectance of an uncoated sample is also shown.

However, it increases to nearly 30% at 0.6 um, which would severely degrade short wavelength performance. Since the long wave performance was acceptable, the spectral curve needed to be shifted to the shorter wavelength. Thus, the stack's optical thickness was adjusted. Figure 18 shows the reflectance for an uncoated reference sample, and a 0.1 um Si_3N_4/0.18 um SiO_2 stack on a Si wafer. The spectral curve was shifted to shorter wavelengths without affecting the long wavelength performance (<10%), but the reflectance increased to 30% between 0.5 um and 0.6 um. Again, the stack's optical thickness needed to be adjusted to improve the short wavelength reflectance. Figure 19 is the reflectance for two samples. The first sample had a 0.094 um Si_3N_4/0.14 um SiO_2 stack, and the second sample had a 0.11 um Si_3N_4/0.12 um SiO_2 thick stack. The former stack had the best short wavelength performance, and nearly identical long wavelength performance. Sample 1 had less than 13% Fresnel reflectance across the 0.5 um to 1.7 um wavelength regime. Recall that the first order estimate was a quarter wavelength thick layer at a central wavelength of 0.75 um which corresponds to this sample. From this analysis, the optical thicknesses were selected for the active area of the detectors. The Si_3N_4 film had a thickness equal to 0.1 $\pm$ um 0.05 um, and a SiO_2 film thickness equal to 0.14 um $\pm$ 0.07 um. The completed photodiode with the two layer AR coating was evaluated. Its spectral responsivity will be discussed in a later section.

Figure 18. Fresnel reflectance of a 2 layer AR coating on Si; Fresnel reflectance of an uncoated sample is also given.

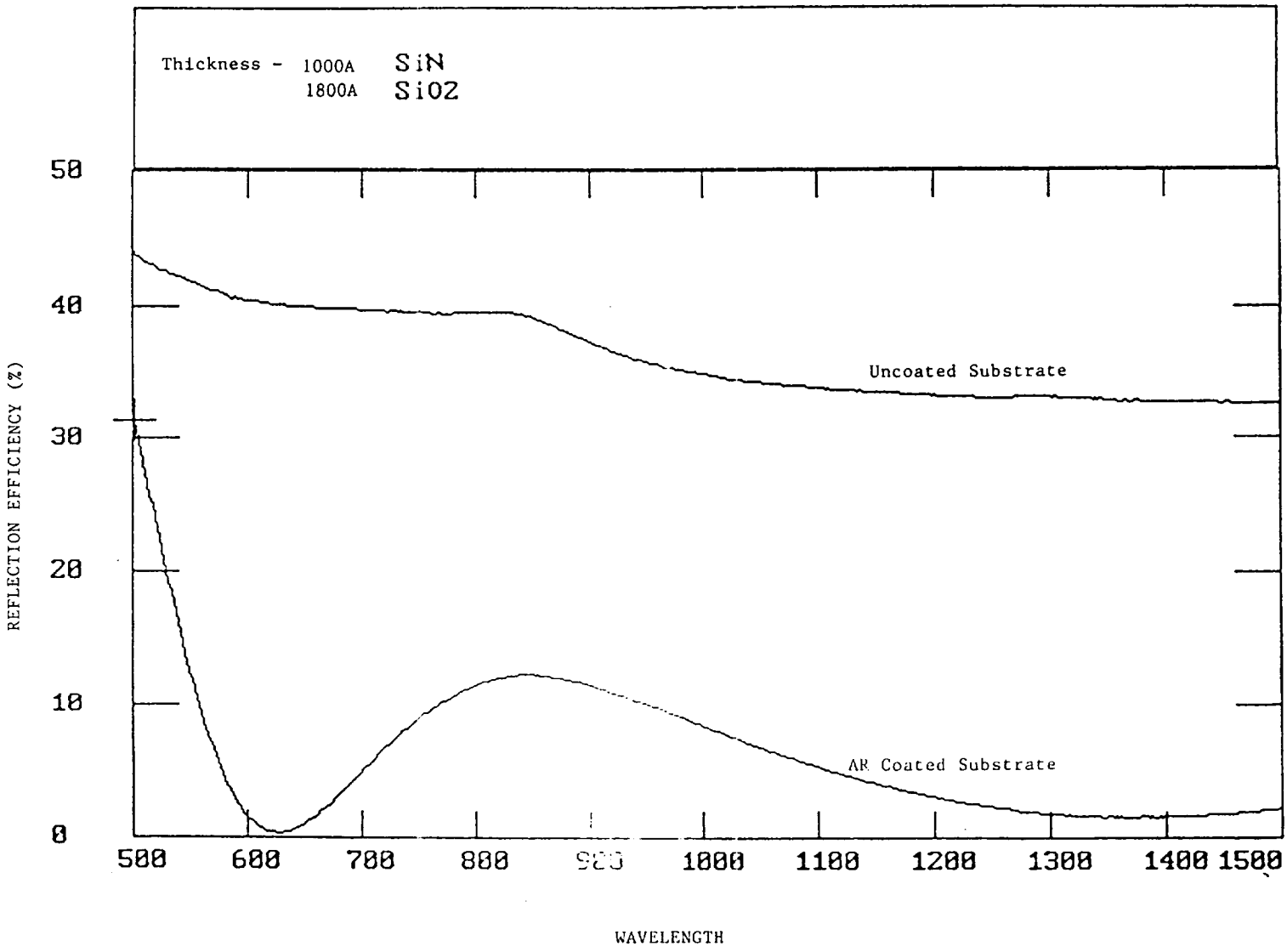

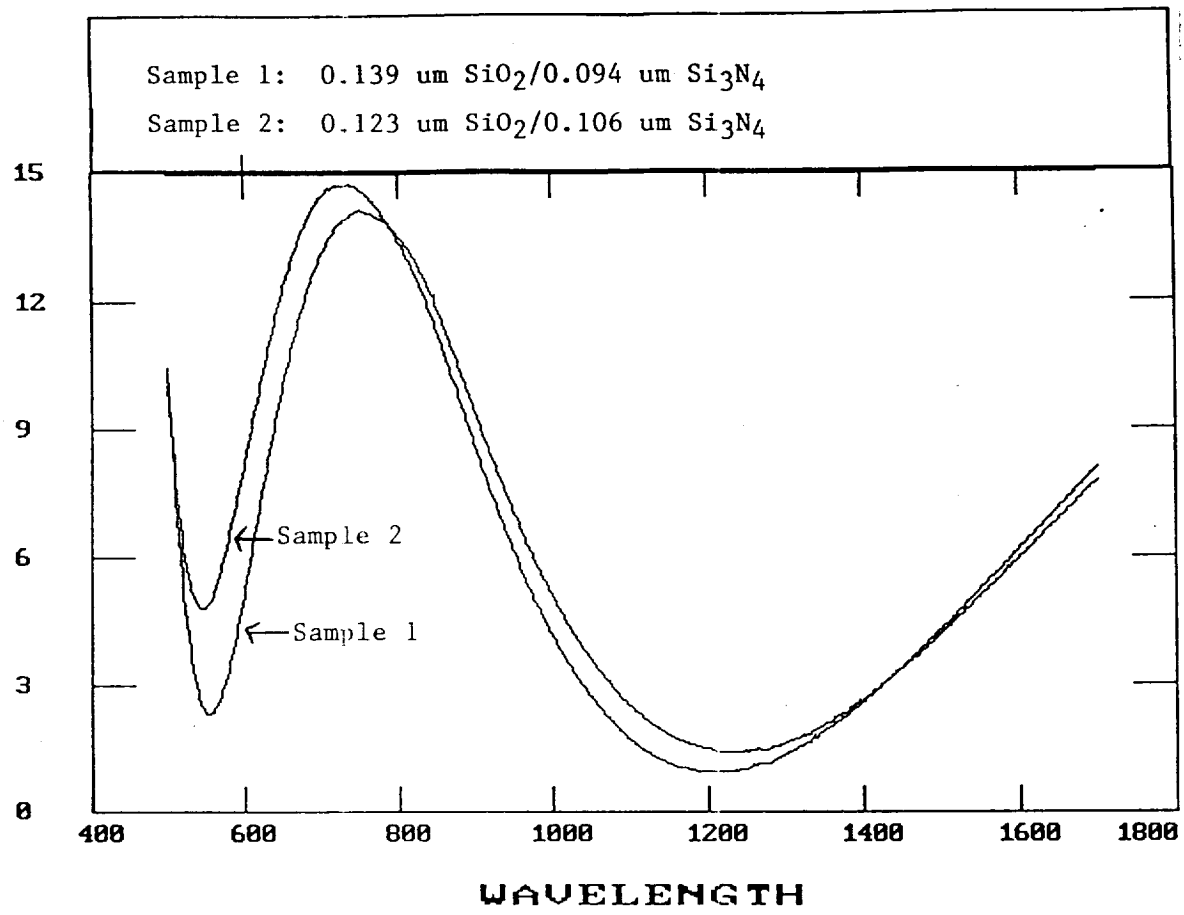

Figure 19. Fresnel reflectance of optimized 2 layer AR coatings.

Curve 1 - 0.094 um Si_3N_4 + 0.14 um SiO_2

Curve 2 - 0.11 um Si_3N_4 + 0.12 um SiO_2

c) Processing sequence

Figure 20 is the block diagram of processing sequence leading to the complete device, i.e. CH_4/H_2 etched, 2 layer AR coated 5 mm active diameter detector, responding in the 0.5 - 1.7 um spectral range. A brief description of these steps follows.

Figure 20. Processing sequence for the production of a plasma etched, 2 layer AR coated detector.

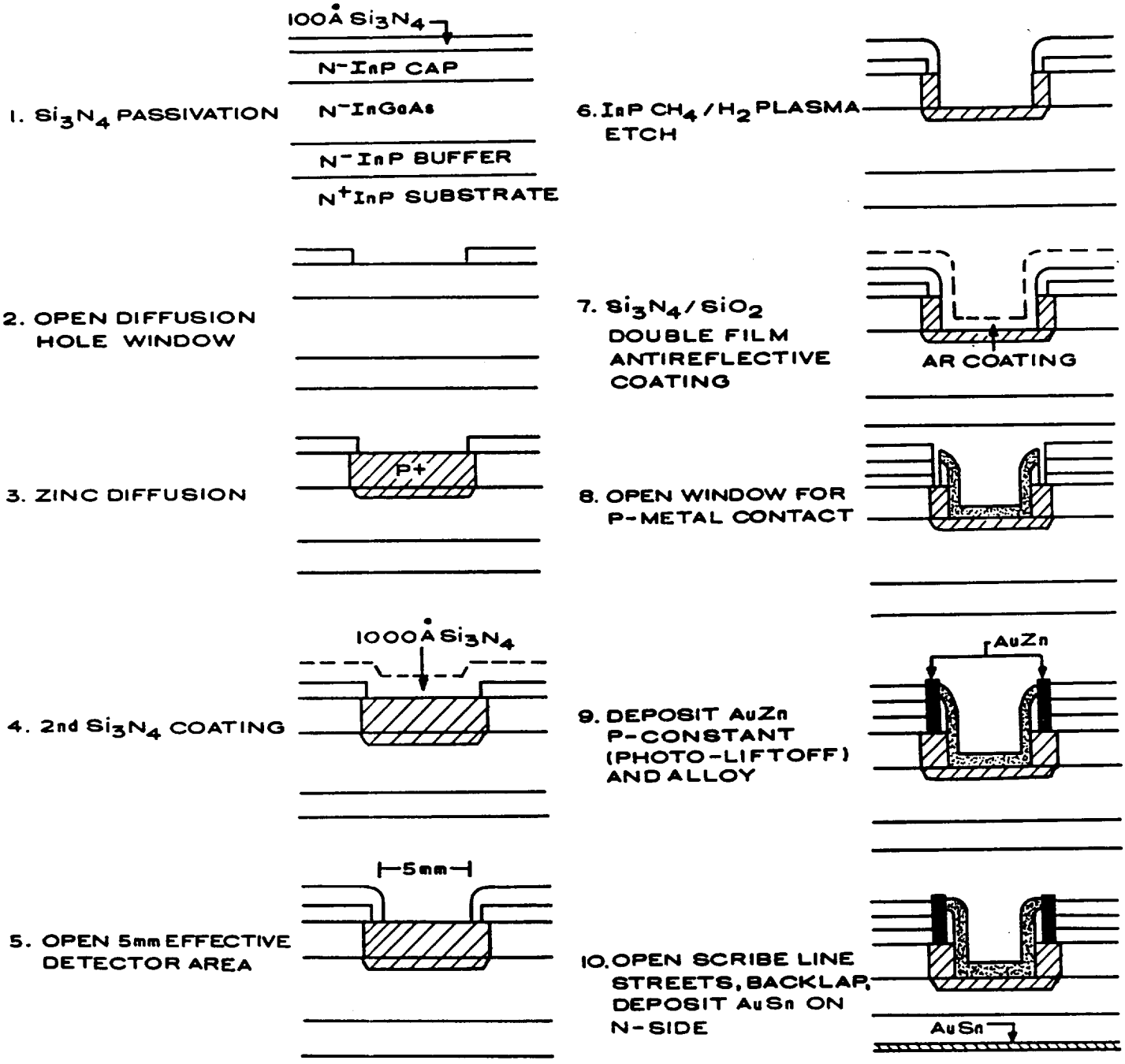

1. After epitaxial growth, 1,000A of SiN_x is deposited on top of the InP cap layer by Plasma Enhanced Chemical Vapor Deposition (PECVD). The SiN_x layer serves as a diffusion mask.

2. A 5.05 diameter window is opened photolithographically on the SiN_x surface, the SiN_x is etched in CF_4/O_2 plasma. Through this window, zinc will be diffused to form the P-N junction of the active detector.

3. The detectors are then diffused with zinc in a sealed, evacuated ampoule using Zn_3As_2 as the diffusion source. The ampoule containing the detectors and diffusion source is annealed at 500^0C for a specified time calibrated to place the P-N junction ~3,000A below the InP cap-InGaAs interface. The P-N junction placed in this position ensures both good quantum efficiency and good device reliability.

4. After the diffusion, the detectors are coated again with 1,000A of SiN_x. This layer serves as a mask which will define the 5 mm broad wavelength response active area.

5. A second photolithography step is used to open a 5.00 mm diameter window concentric to the 5.05 mm diameter diffusion window described above. Then the SiN_x in the 5.00 mm diameter window is etched away in CF_4/O_2 plasma.

6. The InP cap is removed from the 5.00 mm diameter window by reactive ion etching with CH_4/H_2.

   This process etches the InP uniformly without changing the morphology of the original InP surface. It is necessary to remove the InP cap in the detector active area in order to expand the detector spectral response down to 0.5 um.

7. A double layer anti-reflective coating is deposited over the entire detector area. The first layer is 1,000A of SiN_x which has an index of refraction, n = 2.00. The second layer is 1370 A of PECVD SiO_2 with n = 1.46. This double film AR coating structure reduces reflectance to < 10% over the spectral range of 0.5 - 1.7 um.

8. Next, a photolithgraphy step is performed to open a 25 um wide ring around the 5 mm detector active area above the InP cap layer which was zinc diffused but not etched away in Step 6. The AR coating and underlying SiN_x layer within the 25 um ring are then etched away in CF_4/O_2 plasma, leaving the remaining zinc-diffused InP cap layer exposed.

9. Before removing the photoresist which was deposited in step 8, 3,000A of AuZn is thermally evaporated over the entire detector surface. The detectors are then soaked in acetone to "lift-off" the photoresist so that the AuZn remains only on the zinc-diffused InP surface which was left exposed prior to this step. The AuZn is then alloyed at 425^0C for one minute in a N_2/H_2 atmosphere to form an ohmic contact with the InP surface.

NOTE: One purpose the InP cap serves is to isolate the alloyed P-contact from the P-N junction located 3,000A below the InP cap-InGaAs interface. If the AuZn was placed directly on the InGaAs active area, the AuZn would migrate to the P-N junction during the alloying step causing catastrophic detector failure.

10. A final photolithography step is performed to open streets between detectors for subsequent scribing. The detectors are then back lapped to be approximately 125 um thick, and 1,000A of AuSn is thermally evaporated onto the back of detectors to form N-side ohmic contacts.

Figure 21 shows a sequence of photolithographic masks used to carry out the above process. Figure 22 shows the wafer in various stages of processing.

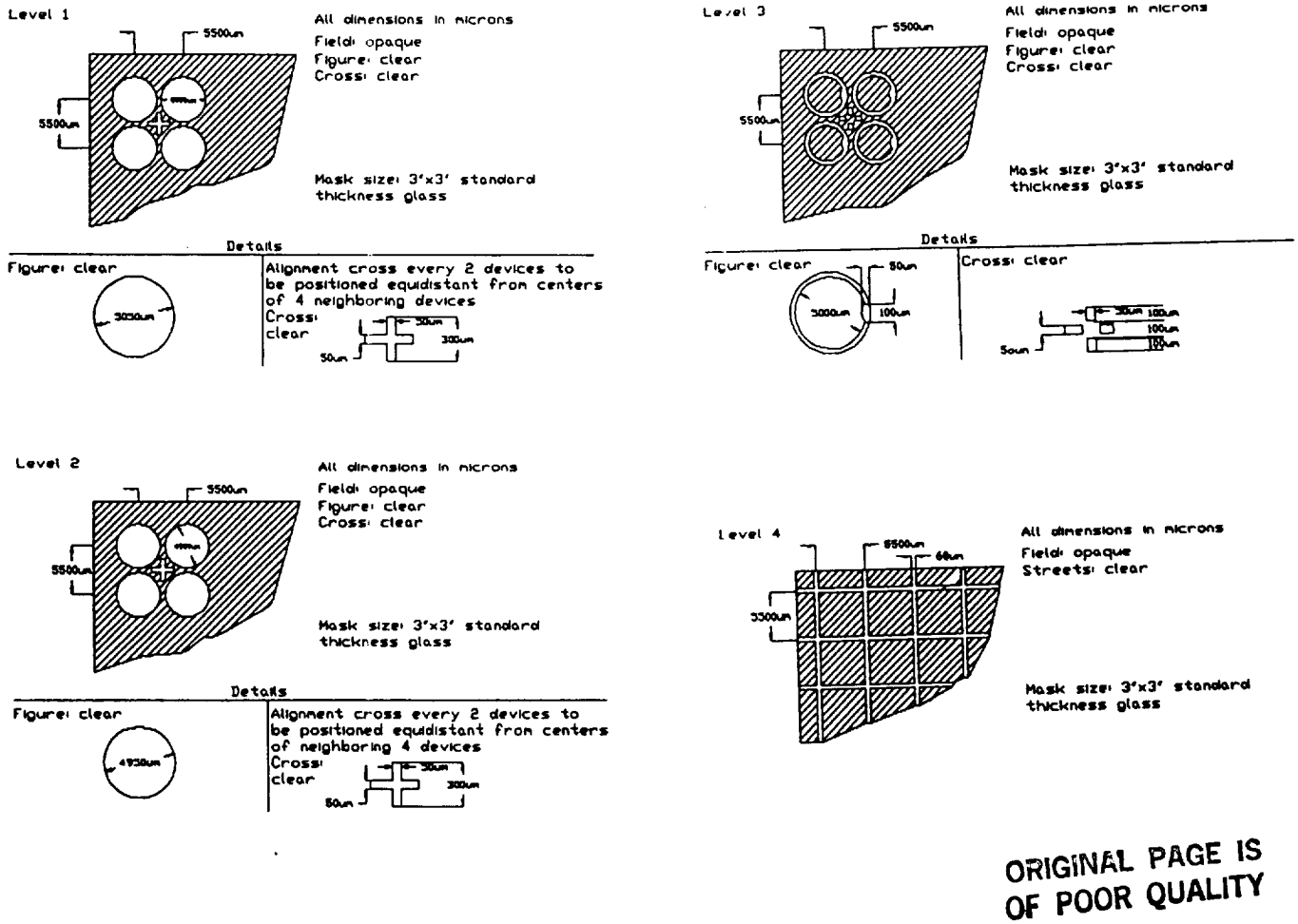

ORIGINAL PAGE IS OF POOR QUALITY

Figure 21. Sequence of photolitographic masks used in the processing.

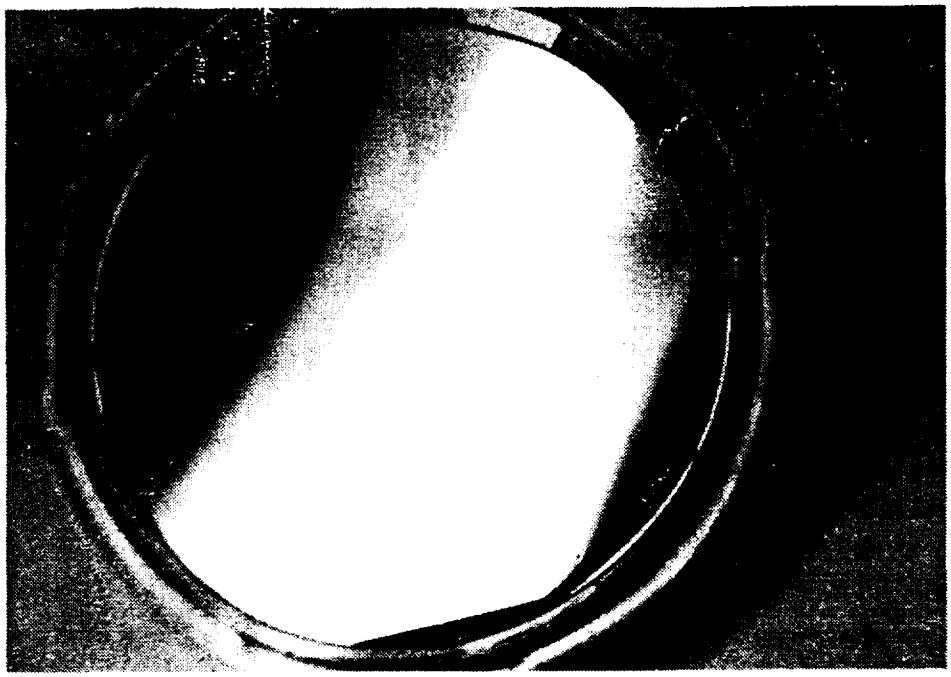

Figure 22a. Photo of the wafer in beginning stages.

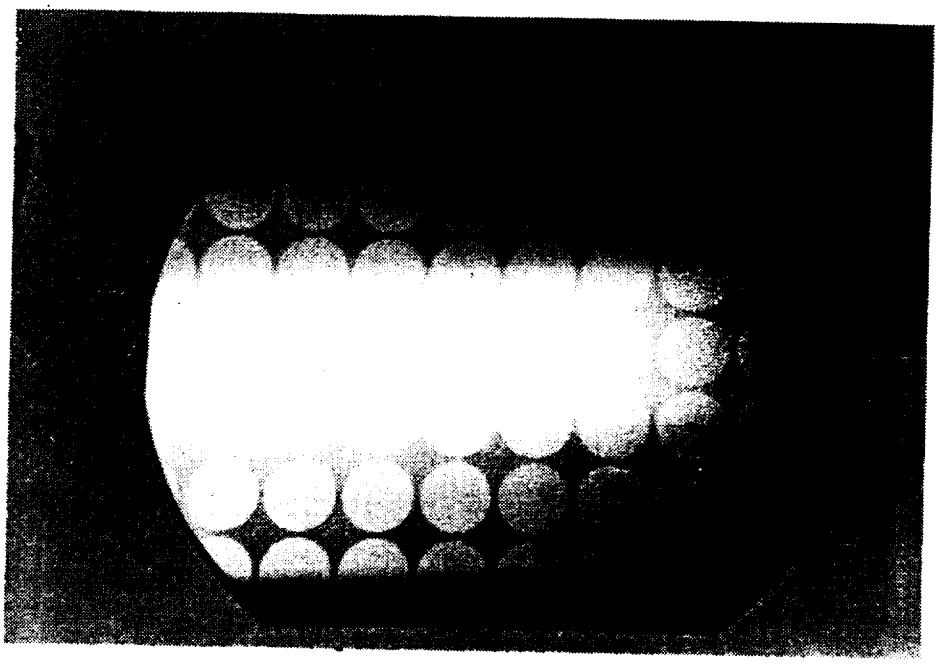

Figure 22b. Photo of the wafer after CH_4/H_2 etching.

d) Wafer Testing

In addition to making 5 mm devices, we also used wafers produced in the new reactor to make smaller diameter devices. These devices were then subjected to testing on an automated wafer tester which, in a step and repeat fashion, tests each device on the wafer. The following parameters are measured: dark current, shunt resistance, responsivity, capacitance and contact resistance. Each device is evaluated with the pass/fail criteria for the above parameters. The associated software then creates maps of the passed or failed devices. Failed devices are ink marked for subsequent discard. Figure 22c shows a pass/fail map for some 700 devices, 1 mm active diameter. One can see that certain parts of the wafer have very high yields, while the other areas were poor. The outline of the 2" wafer and the direction of the gas flow in the VPE reactor is marked. The leading edge has much lower yield. Such information can be used for the further optimization of the epitaxial growth conditions, because it directly connects the yield of devices with epi growth conditions.

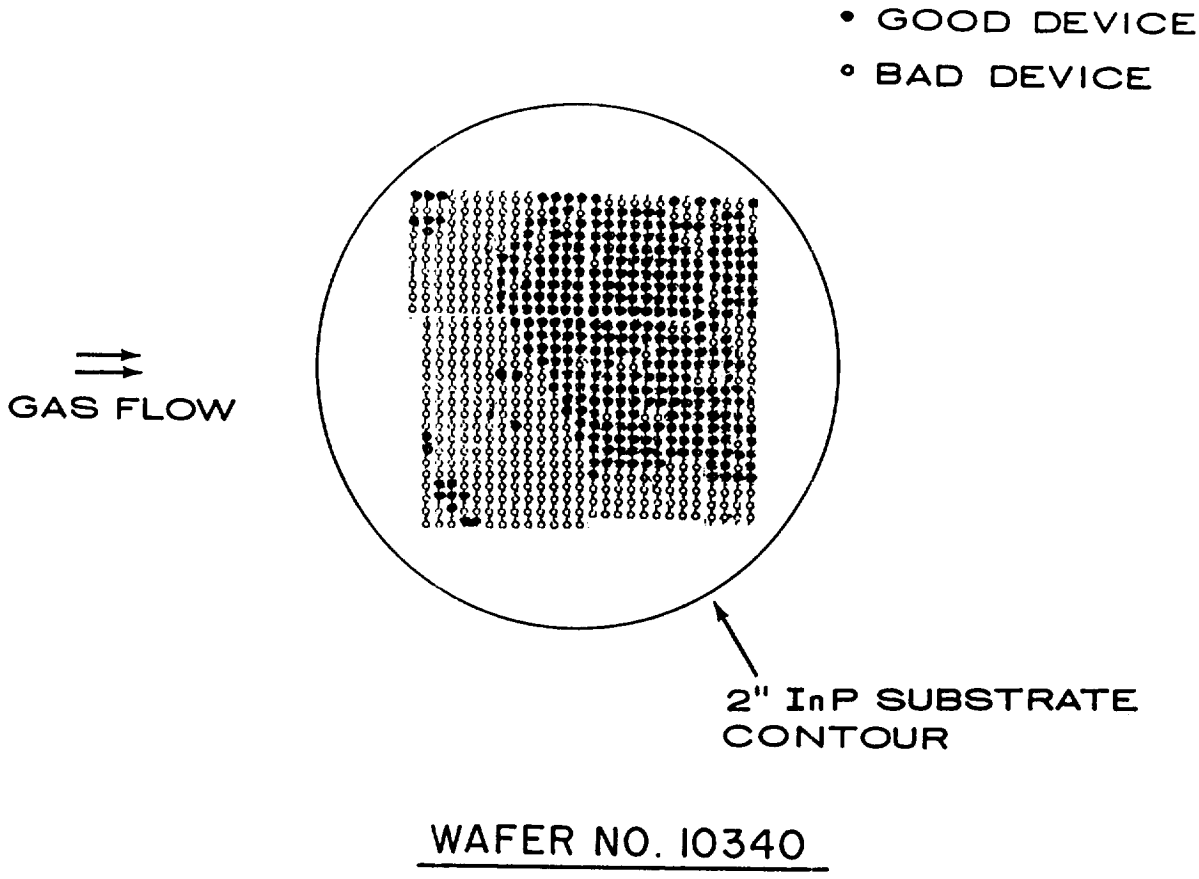

Figure 22c. Wafer testing map showing areas of good and bad 1 mm diameter devices.

The typical values of measured parameters for the mapped wafer (No. 10340) were:

R_{sh} = 5 - 100 MΩ
R > 0.8 A/W
C(-1V) = 65 - 95 pF

These numbers met or exceeded values for devices produced in standard reactors, thus demonstrating the satisfactory performance of the new reactor.

VI. Device packaging

After the testing just described, the wafer is scribed and cleaved along the scribe marks. The chips which passed wafer testing criteria are then selected for the subsequent packaging operation.

The first step in packaging is chip mounting, using either AuSn preform or conductive epoxy. Due to the fragility of 5 mm chips, we used epoxying, which is a less harsh operation than AuSn mounting. Care must be taken to center the chip properly on the base of the 2-pin TO type package. In this operation, the n-side contact is connected to the cathode of the package. The next operation is a thermocompression wire bonding, using 18 um gold wire. In this operation, the p-side contact is connected to the anode lead of the package.

Two quality control operations are performed after mounting and bonding; these are chip shear test and the wire bond pull test.

The next operation is cap sealing, where the package windowed cap is welded to the base to provide hermetic packaging of the detector. After the hermeticity testing, devices are ready for electrical and reliability testing.

The TO package used for 5 mm detectors is shown in Figure 23a, and in Figure 23b, finished devices are shown..

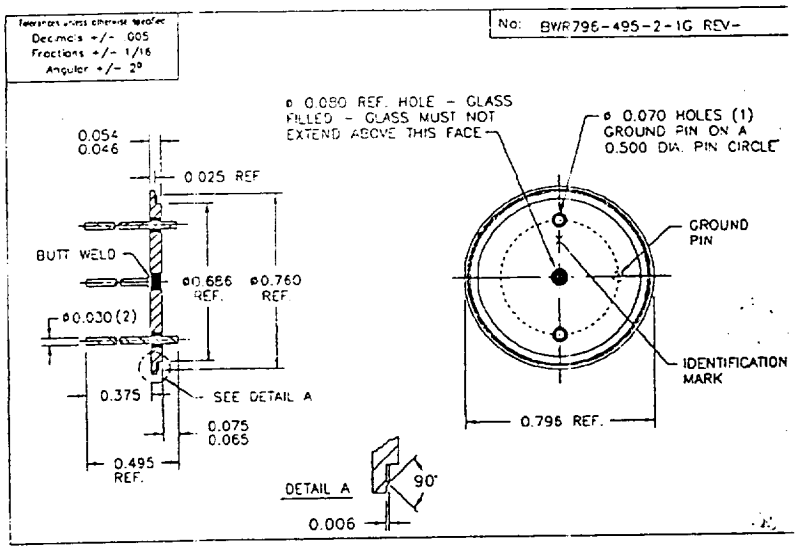

Figure 23a. TO package used for 5 mm detectors.

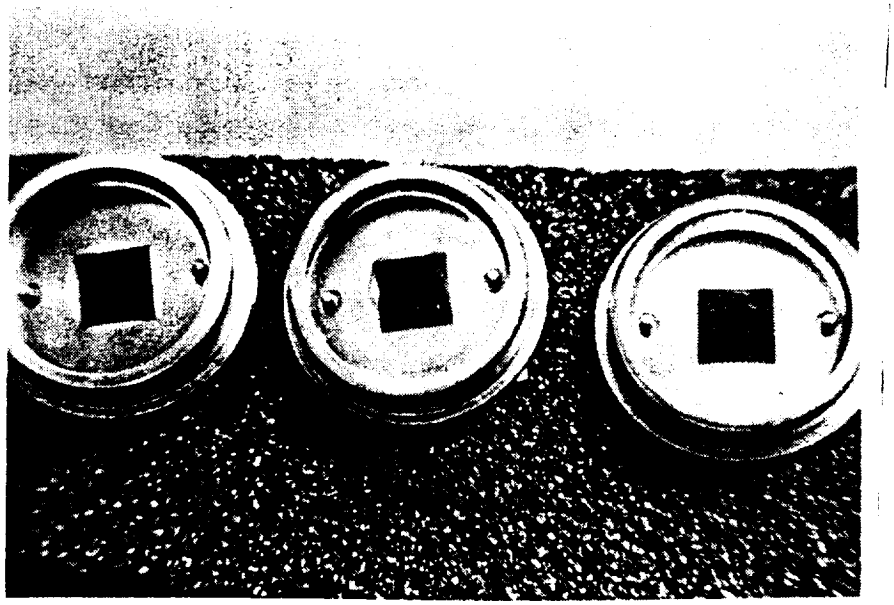

Figure 23b. Finished 5 mm diameter detectors.

VII. Detector testing and performance

After packaging devices are ready for electronic and optical testing.

a) Electronic testing

Dark current and capacitance

Electrical measurements performed on the detectors include I-V (reverse and forward bias) and C-V (reverse bias). Figure 24 illustrates the automated I-V/C-V evaluation station. This is a computer aided measurement station for the following diode parameters: shunt resistance, breakdown voltage, leakage current, series resistance (bulk and contact), depletion depth, carrier concentration and built-in voltage. A Keithley picoammeter is used to monitor the dark current (often at the picoamp level) as a function of applied voltage. A Boonton capacitance meter measures capacitance down to 0.01 pF.

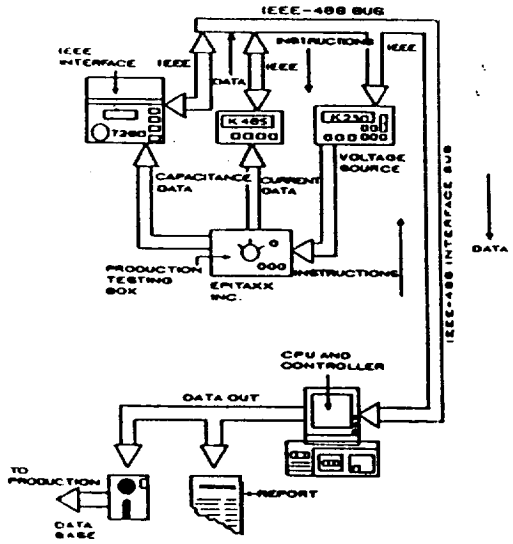

Figure 24. I-V/C-V system for detector characterization.

Figure 25a shows the forward and 25b shows the reverse bias I-V characteristics of a 5 mm device (Note different scales on these graphs).

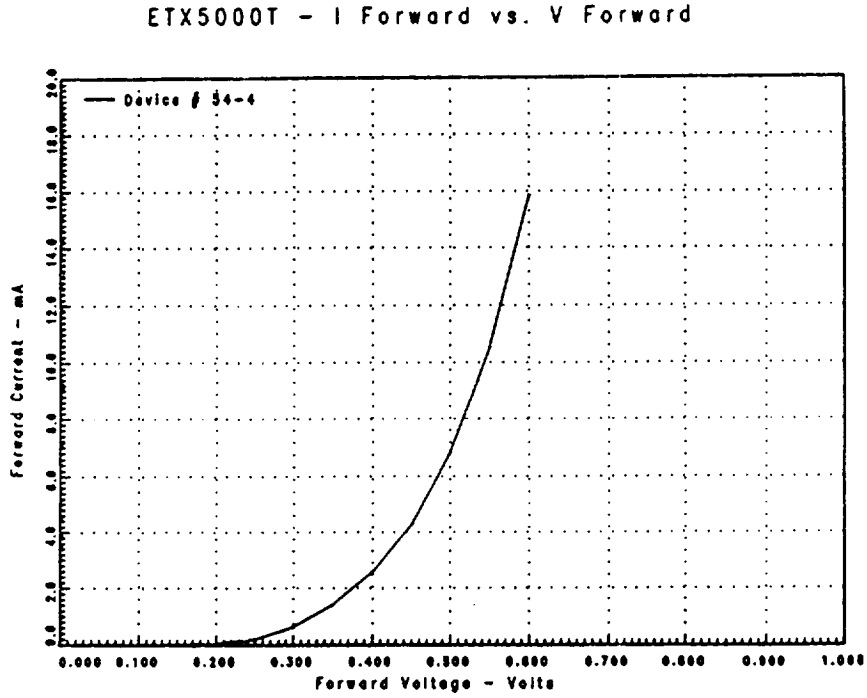

Figure 25a. Forward bias I-V characteristic of 5 mm detector.

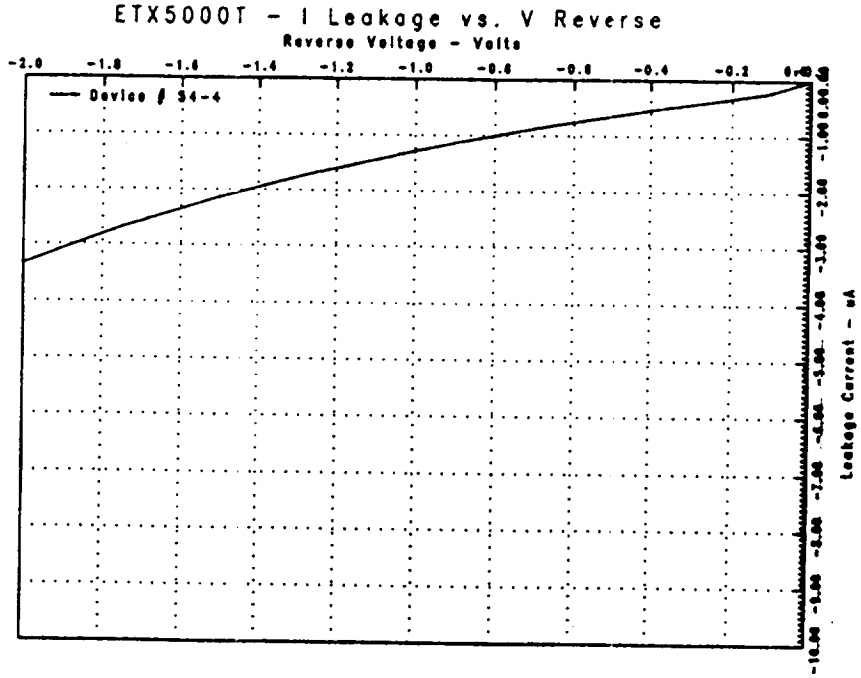

Figure 25b. Reverse bias I-V characteristic of 5 mm detector.

Shunt resistance measurements

Shunt resistance (R_{sh}) is defined as the slope of the current voltage curve at zero bias. Figure 26 illustrates the test station. The device under test is inserted into a light tight enclosure. A computer controlled voltage source applies forward and reverse bias in 1 millivolt increments to 10 millivolts. The internally generated current is recorded, and the slope (defined as the shunt resistance) is calculated.

$$i_j^2{}_n = 4\ kTB/R_{sh}$$

k = Boltzman's constant
T = absolute temperature
B = bandwidth

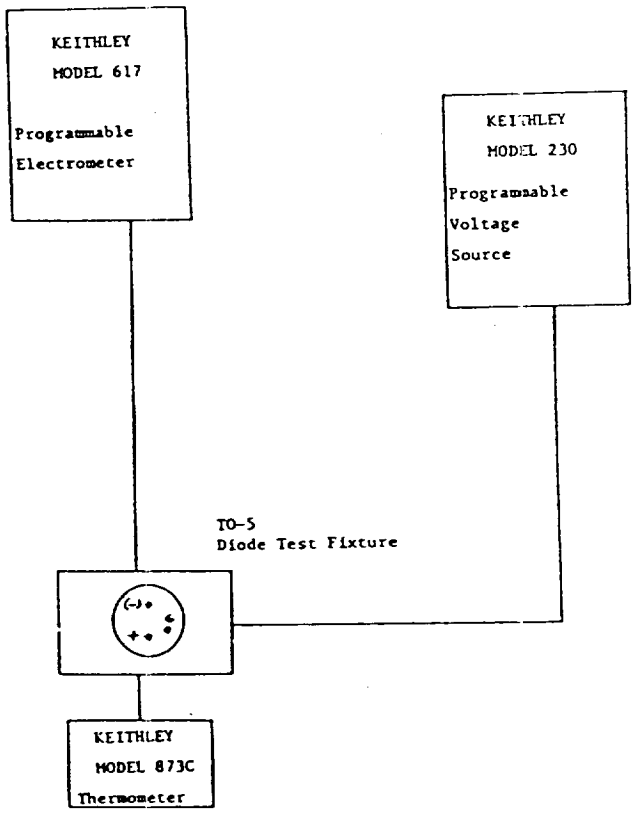

Figure 26. Test station for shunt resistance measurements.

Rise time measurements

Rise/fall time measurements have also been performed on these large-area InGaAs detectors to determine their potential speed of operation. A 1300 nm pulsed laser (with a rise time below 2 nsec) is used as a radiation source to the large area detector. The shape of the resultant current pulse is used to determine rise/fall time of the detector.

b) Optical testing

Spectral responsivity

Discrete and continuous spectral efficiency measurements were completed for the photodiodes. Discrete wavelength measurements were completed on all deliverables, and a 500 nm to 1000 nm scan was completed on a sample unit. A 0.6328 um He-Ne laser, a 0.85 um AlGaAs LED, and a 1.3 um InGaAsP LED were used as the discrete sources. Figure 27 illustrates the test station. A WDM coupler was integrated into the two LED's to provide a single fiber delivery system. The He-Ne laser was coupled to a second fiber to allow fiber optic injection into the test diodes. Calibrated Si (for the visible spectrum), and InGaAs (for the near infrared spectrum) provided the reference input power used in calculating absolute responsivity. The appropriate fiber was micropositioned to the test photodiode, and its projected spot illuminated approximately 60% of the diode's active surface diameter. The output photocurrent from the test diode is recorded, and the packaged device responsivity is calculated. Table 3 lists the device responsivity for the deliverable 5 mm diameter photodiodes. These values include the glass window's Fresnel transmission loss (approximately 8%). The photodiode's responsivity is used to calculate its external quantum efficiency (EQE) which is expressed by 1.24 R / WL, where R is the responsivity (A/W), and WL is the wavelength (um). Also, a standard EPITAXX photodiode is included to illustrate their differences. Figure 28 is the relative spectral responsivity from .500 um to 1.000 um for a representative sample. It had a maximum response of 0.6 A/W at 0.95 um. This corresponds to a calculated external quantum efficiency between 46% and 78% in the tested range. These high values are achieved through the optimized short wavelength transmittance due to the two layer AR coating, and the substantially reduced InP cap thickness (nearly a factor of 10).

Figure 27. Test station for measuring detector responsivity at discrete wavelengths (0.63, 0.85 and 1.30 um), and a spectral response uniformity.

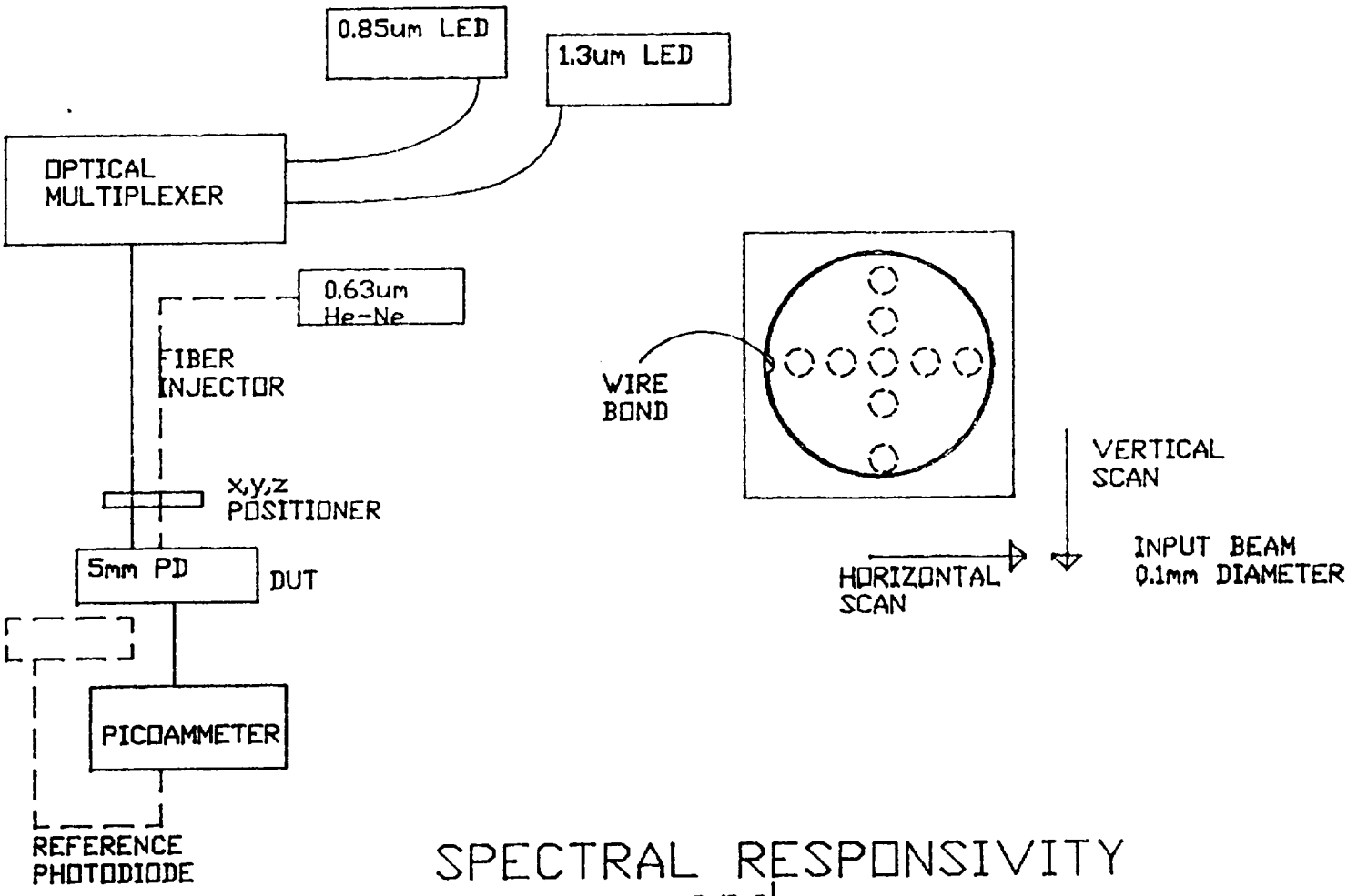

Spectral response uniformity

A surface uniformity scan was performed on a sample diode to measure changes in spectral response - indicating a possible taper in the depletion width and/or InP cap layer (the cap layer would affect short wavelength response). A scanning fiber is used to selectively illuminate the test diode (Figure 27 illustrates the test station). A 1300 nm source was used to generate a surface plot of a sample deliverable. Figure 29 is the resultant plot with 4 views. Some taper is apparent, especially in the rotational views. Its magnitude is approximately ±5 percent. Short wavelength non-uniformities are associated with tapers in the InP cap layer. A He-Ne laser coupled to a fiber was scanned across a sample diode, and a ±10 percent intensity variation was observed across the diode's diameter.

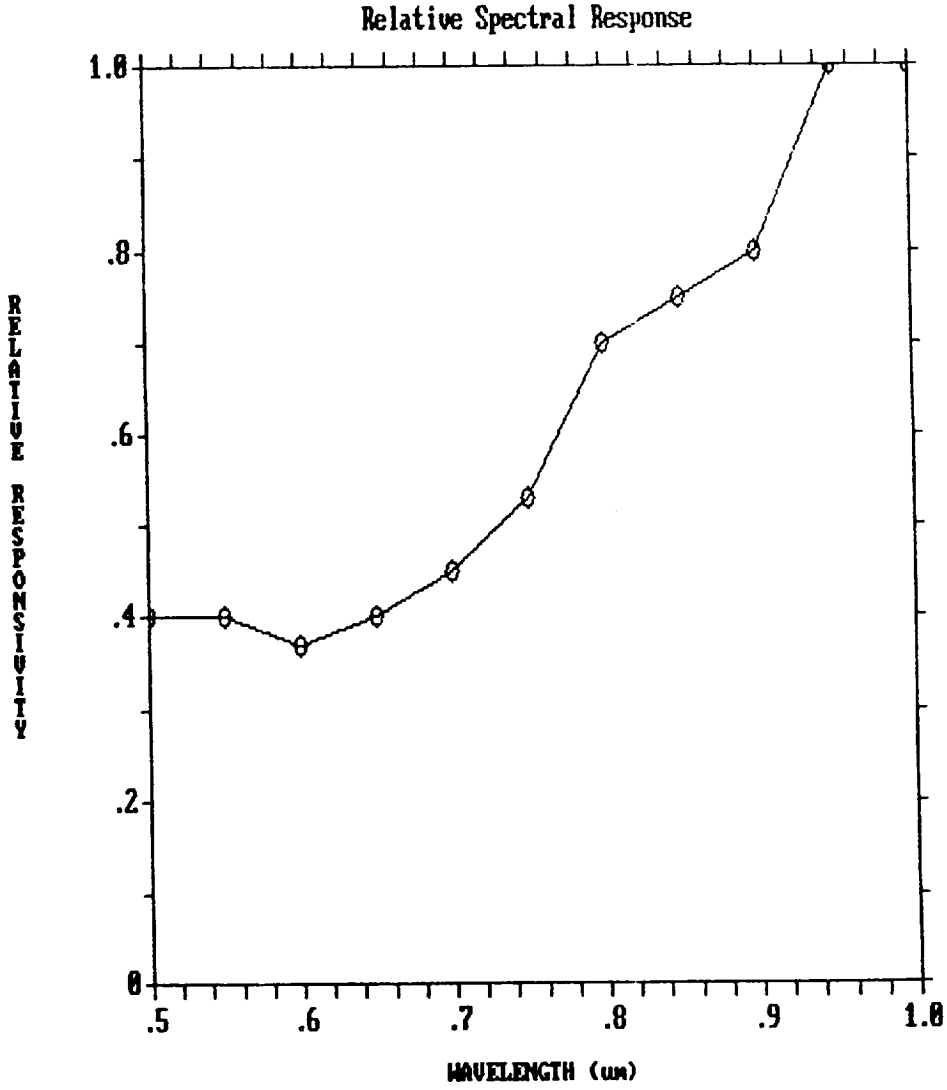

Figure 28. Relative spectral response uniformity plot.

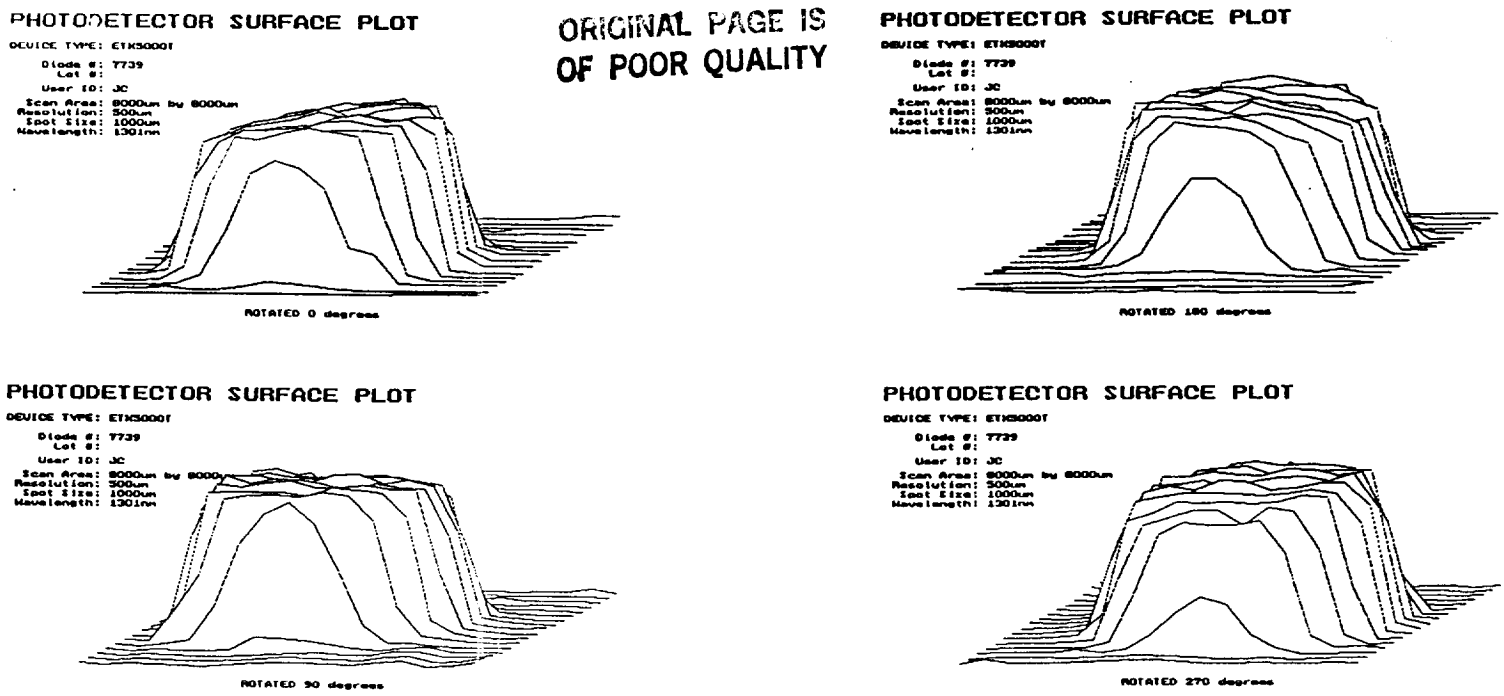

Figure 29. Photodetector spectral response uniformity plot.

c. Operation at elevated temperatures

A high temperature burn-in was completed on several photodiodes from different lots to verify survivability at elevated temperature and reverse bias. The initial photodiode dark current at 25C and reverse bias equal to 10 mV and 1V was recorded. These units were installed in a light tight enclosure and inserted into an oven. The temperature was set to 125C, and the devices were operated at 1V. At the burn-in temperature (125C), the first dark current measurements were made at 10 mV and 1V reverse bias. Subsequently, the diodes were operated at 1 V for 115 hrs., and a final measurement at the bias voltages were made. The results for PD # 3578-1 and PD # 7739-4 before and after the 115 hr. burn-in are:

	BEFORE		AFTER	
	Rsh (10 mV) (Kohm)	Id (1V) (uA)	Rsh (10 mV) (Kohm)	Id (1V) (uA)
PD#3578-1	58.1	16.5	75.8	14.5
PD#7739-4	285.7	3.3	312.5	3.4

These devices not only survived the burn-in, but the electrical performance improved.

Figure 30 shows the results of in-situ measurements of dark current of photodiodes at 125C. These devices had a decrease in the leakage current over the 115 hr. test period, when measured either at -1V or at -10mV. We thus conclude that 5 mm InGaAs are capable of operation at elevated temperatures (+125C).

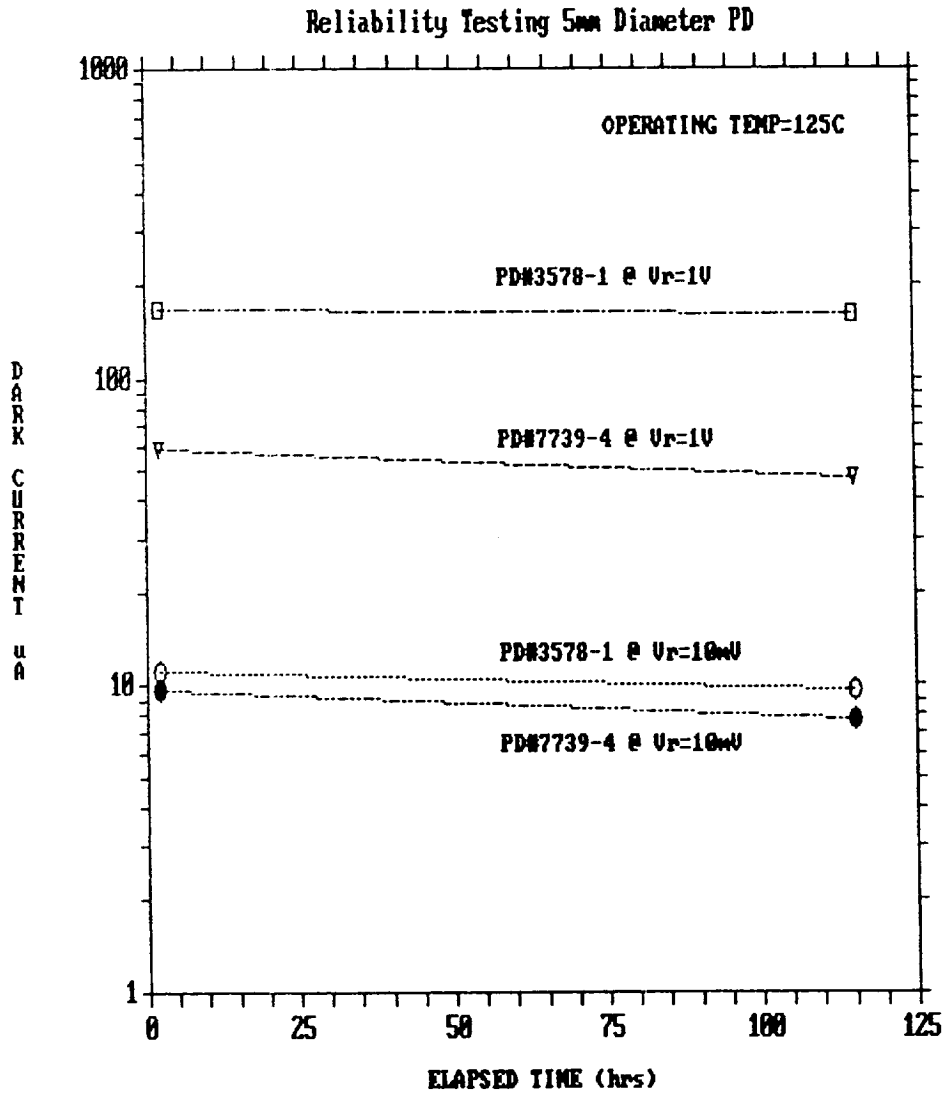

Figure 30. Results of the in-situ measurements of dark current of detectors maintained at 125C (curves for bias of -1V and -10 mV are shown).

d. Detector performance

Table 3 summarizes the results of the electronic and optical characterization of detectors delivered to the contractor. The following parameters are listed: shunt resistance, dark current (@ -1V), capacitance (@ 0V and -1V), responsivity at 0.633, 0.850 and 1300 um and quantum efficiency at these wavelengths. For comparison, responsivity and quantum efficiency (QE) of a standard InGaAs detector (i.e. devices without special AR coating and CH_4/H_2 plasma well etching) are also listed.

Table 3. Summary of electronic and optical characterization of 5 mm InGaAs detectors delivered to the contractor.

Device	Rsh (Kohm)	Id(-1V) uA	C (0V) pF	C (-1V) pF	R (0.633um) A/W	R (0.850um) A/W	R (1300um) A/W	QE (0.633 um) (%)	QE (0.850 um) (%)	QE (1.300 um) (%)
Lot # 3578										
1	68.9	nm	1516	1253	0.15	0.34	0.85	0.32	0.54	0.88
2	69.9	nm	1471	1193	0.19	0.41	0.84	0.40	0.65	0.87
3	25.0	nm	1351	1201	0.12	0.30	0.84	0.26	0.48	0.87
Lot # 10349										
1	76.9	28.6	1281	1273	0.19	0.33	0.76	0.40	0.52	0.79
2	18.5	110.0	1257	1305	0.14	0.30	0.70	0.30	0.48	0.73
3	217.4	1.4	1592	1529	0.17	0.31	0.72	0.36	0.49	0.75
Lot # 7739										
1	80.0	27.0	2337	1691	0.21	0.31	0.69	0.45	0.49	0.72
2	44.0	184.0	1450	1313	0.27	0.29	0.84	0.58	0.46	0.87
3	303.0	3.15	2330	1666	0.20	0.30	0.68	0.43	0.48	0.71
4	96.0	44.0	nm	nm	0.24	0.32	0.75	0.51	0.51	0.78
Standard	--	--	--	--	0.08	0.20	0.88	0.17	0.29	0.91

nm = not measured

The speed of response was also measured with a set up previously described:

At 0 V bias: rise time t_ρ = 632 ns
fall time t_ϕ = 550 ns
At -1 V bias: rise time t_ρ = 296 ns
fall time t_ϕ = 302 ns

The load resistance was 50 W and the laser power (1.3 um wavelength) was 400 uW.

Contact resistance was also measured; it was found to vary between 17 and 33 ohms, the median value being 24 ohms.

VIII. Summary and Conclusions

In the course of this work, we produced 5 mm diameter InGaAs pin detectors which met or exceeded all of the goals proclaimed at the onset of the program.

The best results achieved were:

* Shunt resistance of over 300 K ohms
* Rise time of less than 300 ns
* Contact resistance of less than 20 ohms
* Quantum efficiency of over 50% in the 0.5 - 1.7 um range
* Devices were maintained and operated at 125^{o}C for over 100 hours without degradation

The above values met or exceed the goals of the program. Ten operational, fully characterized detectors are delivered with this report.

In order to achieve the goals of this program, several major technological advances were realized, among them:

* Successful design, construction and operation of a hydride VPE reactor capable of growing epitaxial layers on 2" diameter InP substrates with a capacity of over eight wafers per day

* Wafer processing was upgraded to handle 2" wafers

* Method for depositing 2 layer Si_3N_4/SiO_2 antireflection coating which enhances response over the 0.5 - 1.7 um range was developed.

* Method for anisotropic, precisely controlled CH_4/H_2 plasma etching for enhancement of response at short wavelengths was developed.

* Electronic and optical testing methods were developed to allow full characterization of detectors with novel size and spectral response characteristics.

On the basis of the work and results achieved in this program, we conclude that large size, high shunt resistance, high quantum efficiency InGaAs pin detectors are not only feasible but also manufacturable on industrial scale. This novel device spans a significant portion of visible and near infrared spectral range and it will undoubtedly find many useful applications.

IX. Acknowledgement

This work was carried out with financial support of NASA, which EPITAXX, Inc. gratefully acknowledges. Many people at EPITAXX contributed to the successful conclusion of this program. Overall direction was provided by V.S. Ban and G.H. Olsen. G. Erickson, D. Rodefeld and D. Ackley were in charge of epitaxy, K. Woodruff and M. Lange of processing and G. Gasparian, J. Colosi, J. Spadafora and J. Rue characterized devices.

We also acknowledge and greatly appreciate contributions made by Prof. Tim Anderson of the University of Florida (vapor phase epitaxy) and Profs. Jim Palmer (internal quantum efficiency) and Angus McCloud of the University of Arizona, Optical Sciences Center (antireflection coatings).

X. Deliverables

Ten detectors with characteristics given in Table 3 were delivered to NASA.

XI. References

1. G.H. Olsen and V.S. Ban, "InGaAsP: The Next Generation in Photonics Materials", Solid State Technology, 30, 99 - 105 (1987).

2. V.S. Ban, M. Popov, G. Erickson, F.D. Speer, D. Gay and G.H. Olsen, "VPE Growth of InGaAs for Large Area and Extended Spectral Range Photodetectors", Proceedings of the SPIE, Vol. 722, p. 192 (1986).

3. G.H. Olsen and T.J. Zamerowski, "Double Barrel III-V Compound Vapor Phase Epitaxy Systems", RCA Review 44, 270 - 286, (1983).

4. V.S. Ban, "Novel Reactor for High Volume, Low-Cost Silicon Epitaxy", J. Crystal Growth, 45, 97 - 107, (1978).

5. C.H. Park, V.S. Ban, T.J. Anderson, G.H. Olsen, "Materials and Detectors Based on $In_{.53}Ga_{.47}As$ Grown by the New Vapor Phase Epitaxy (VPE) Technique Utilizing In/Ga Alloys", submitted for publication to J. Electron. Materials.

6. U. Niggebrugge, M. Klug and G. Garus, "A Novel Process for Reaction Ion Etching of InP Using CH_4/H_2", Inst. Phys. Conf. Ser. No. 79, Chapt. 6, pp. 367, A. Hilger, Bristol, U.K. (1985).

7. D. Johnson and C. Constantine, Oral Communication, Plasmatherm, Inc., Kresson, New Jersey.

NASA National Aeronautics and Space Administration

Report Documentation Page

1. Report No.	2. Government Accession No.	3. Recipient's Catalog No.

4. Title and Subtitle

"Development of a Unique Laboratory Standard Indium Gallium Arsenide Detector for the 500 - 1700 um Spectral Region"

"NASA Phase II Final Report"

5. Report Date

June 5, 1990

6. Performing Organization Code

7. Author(s)

Dr. Vladimir S. Ban, Executive Vice President & COO

Dr. Gregory H. Olsen, President & CEO

8. Performing Organization Report No.

10. Work Unit No.

9. Performing Organization Name and Address

EPITAXX, Inc.
3490 U.S. Route One
Princeton, New Jersey 08540

11. Contract or Grant No.

NAS5-30312

13. Type of Report and Period Covered

Final Report

12. Sponsoring Agency Name and Address

NASA Goddard Space Flight Center
Greenbelt Road
Greenbelt, Maryland 20771

14. Sponsoring Agency Code

15. Supplementary Notes

None

16. Abstract

In the course of this work, we produced 5 mm diameter InGaAs pin detectors which met or exceeded all of the goals proclaimed at the onset of the program.

The best results achieved were:

* Shunt resistance of over 300 K ohms
* Rise time of less than 300 ns
* Contact resistance of less than 20 ohms
* Quantum efficiency of over 50% in the 0.5 - 1.7 um range
* Devices were maintained and operated at 125°C without deterioration for over 100 hours

The above values meet or exceed the goals of the program. Ten operational, fully characterized detectors are delivered with this report.

17. Key Words (Suggested by Author(s))	18. Distribution Statement
InGaAs detector	

19. Security Classif. (of this report)	20. Security Classif. (of this page)	21. No. of pages	22. Price
		48	

NASA FORM 1626 OCT 86